Government of **Western Australia**
Department of **Mines and Petroleum**

RECORD 2009/24

AGE CONSTRAINTS AND STRUCTURE OF THE COHN HILL SHEAR ZONE, WESTERN MUSGRAVE BLOCK, WESTERN AUSTRALIA

by
A Sen




THE UNIVERSITY OF ADELAIDE AUSTRALIA

Geological Survey of Western Australia

NGAANYATJARRA COUNCIL (Aboriginal Corporation)

Government of Western Australia
Department of Mines and Petroleum

Record 2009/24

AGE CONSTRAINTS AND STRUCTURE OF THE COHN HILL SHEAR ZONE, WESTERN MUSGRAVE BLOCK, CENTRAL AUSTRALIA

by
A Sen

Tectonics, Resources and Exploration, Discipline of Geology and Geophysics School of Earth and Evironmental Sciences, University of Adelaide, South Australia

Geological Survey of Western Australia

THE UNIVERSITY OF ADELAIDE AUSTRALIA

NGAANYATJARRA COUNCIL (Aboriginal Corporation)

Notice to the reader
This Record is one of a series of BSc. Hons theses researched, written and compiled by students from the Centre of Tectonics, Resources and Exploration (TRaX), University of Adelaide, through an ongoing collaborative project between the Geological Survey of Western Australia (GSWA) and the University of Adelaide. Although GSWA has provided field and laboratory support for this project, the scientific content of each Record, and the drafting of figures, has been the responsibility of the authors. No editing has been undertaken by GSWA.

All work carried out in the west Musgrave region is done so within the framework of an ongoing collaborative project involving GSWA, the Traditional Owners of the region and the Ngaanyatjarra Council. The considerable efforts of the Traditional Owners and of the Ngaanyatjarra Council in facilitating this work is gratefully acknowledged.

REFERENCE
The recommended reference for this publication is:
Sen, a 2009, Age Constraints and Structure of the Cohn Hill Shear Zone, Western Musgrave Block, Central Australia: Geological Survey of Western Australia, Record 2009/24, 83p.

National Library of Australia Card Number and ISBN 978-1-74168-283-0

Published 2009 by Geological Survey of Western Australia
This Record is published in digital format (PDF) and is available online at www.dmp.wa.gov.au/GSWApublications. Laser-printed copies can be ordered from the Information Centre for the cost of printing and binding.

Further details of geological publications and maps produced by the Geological Survey of Western Australia are available from:
Information Centre
Department of Mines and Petroleum
100 Plain Street
EAST PERTH, WESTERN AUSTRALIA 6004
Telephone: +61 8 9222 3459 Facsimile: +61 8 9222 3444
www.dmp.wa.gov.au/GSWApublications

Age Constraints and Structure of the Cohn Hill Shear Zone, Western Musgraves Block, Central Australia

Alexander Sen

Tectonics, Resources and Exploration
Discipline of Geology and Geophysics
School of Earth and Environmental Sciences
University of Adelaide, South Australia
alexander.sen@student.adelaide.edu.au

Table of Contents

Age Constraints and Structure of the Cohn Hill Shear Zone, Western Musgrave Block, central Australia

Alexander Sen

School of Earth and Environmental Sciences
University of Adelaide

Abstract:

Sensitive High Resolution Ion Microprobe (SHRIMP) U-Pb zircon ages provide key constraints on multiple events spanning the Musgravian Orogeny and the Ngaanyatjarra Rift. The U-Pb SHRIMP zircon crystallisation age of 1135 ± 5.9 Ma from a pegmatite dyke confirms the decompression of the Cohn Hill supracrustal sequence within the limits of the very late Musgravian Orogeny. Simultaneous UHT conditions and sinistral, transpressive shearing existed during decompression yet the extent and timing of this event remains unclear. This important constraint opens a gateway for the detailed metamorphic study of the decompressional assemblages relating to the evolution of the Musgravian Orogeny. Additionally, key field observations record the preservation of Musgravian fabrics oriented orthogonal to the commonly reported north-south structural grain. These fabrics suggest an east-west, sinistral (top plate to east) horizontal detachment mylonite, prior to the development of large scale north-south, tight folds.

Alongside this Mesoproterozoic terrain, a migmatite yields two SHRIMP U-Pb ages: 1160 ± 15 Ma (crystallisation of host) and migmatisation at 1066 ± 5 Ma. Migmatisation is associated with the widespread tectonic and magmatic activity during Phase 3 of the Ngaanyatjarra Rift. Furthermore, the migmatisation age is coincident with significant mineralization associated with the Alcurra dyke suite. Structural relationships and field observations suggest a possible setting for orthomagmatic mineralization to the west of Cohn Hill.

1. Introduction

The basement rocks of the Musgrave Block preserve an extensive record of large-scale deformational events dating from the late Mesoproterozoic to the Neoproterozoic. Felsic gneisses, collectively termed the Wirku Metamorphics, constitute much of the basement of the West Musgrave Complex (Smithies et al., 2008). Their age and nature are poorly constrained however deposition is thought to have occurred between c. 1360 and 1307 Ma, prior to and coincident with the intrusion of the c. 1336 -1293 Ma Wankanki Supersuite (Smithies et al., 2008). Multiple orogenesis and high-grade metamorphism (White et al., 1999), intrusion of felsic, mafic and ultramafic melts as well as long-lived failed rifting (Evins et al., in press), have all left an imprint upon the Wirku Metamorphics.

This study focuses on the Wirku Metamorphics of the Cohn Hill region, where evidence of all the above-mentioned events is present in a high-grade kilometre-scale shear zone. U-Pb Sensitive High Resolution Ion Microprobe (SHRIMP) geochronology and structural mapping aim to constrain the relative timing of local deformation associated with the c.1219 – 1155 Ma. (Smithies et al., 2008) Musgravian Orogeny and Pitjantjatjara Supersuite, as well as the long lived c.1120 - 1040 Ma Ngaanyatjarra Rift and related c. 1075 Giles intrusions. Further outcrop scale strain mapping of the shear zone aims to investigate its evolution and relationship to multiple high-grade orogenesis.

Previous studies on this region by Clarke et al. (1991), Kelly et al. (2006) and Werner et al., (2009) provide invaluable information on the metamorphic history of the area.

2. Geological setting

2.1 Regional geological setting

Central Australia's Musgrave Complex is an early Mesoproterozoic to Neoproterozoic belt geophysically represented by an east-west trending anomaly 800km long and up to 300km wide (Evins et al., in press). Straddling the Northern Territory, South Australia and Western Australia borders and bounded by basins of the former Centralian Superbasin, the Musgrave Complex arrived at its present position by major Neoproterozoic intracontinental deformation (Raimondo et al., 2009).

The basement consists of generally felsic volcanosedimentary and sedimentary gneisses with intrusives in the eastern Musgrave block yielding a crystallization age of c. 1600 Ma (Maboko et al., 1991; Camacho & Fanning, 1995; Edgoose et al., 2004). Wade et al. (2008) suggest that these intrusives originated from an arc setting, which experienced c. 1594 Ma closure and subsequent extension at c. 1400Ma. This extension marks the depositional age of the east Musgrave basement (Wade et al., 2008). On the other hand, the western Musgrave Complex holds no intrusive or extrusive exposures older than c. 1400Ma (Smithies et al., 2008). The minimum depositional age for the west Musgrave basement is restricted to between c. 1360 and 1307Ma, which is before and during intrusion by the c. 1336-1293 Ma. Wankanki Supersuite (Smithies et al., 2008). Several studies have attempted to divide the basement gneisses (Collectively known as the Wirku Metamorphics) into definitive age groups (Sun & Sheraton, 1992; Camacho & Fanning, 1995; Sun et al, 1996; White et al., 1999; Edgoose et al., 2004; Wade et al., 2006; Smithies et al., 2008;). Smithies et al. (2008) defines at least four geographically separate groups of Wirku metamorphics based on age spectra of detrital zircons. However,

relationships between them do not rule out a singular depositional basin evolving between c. 1360 and c. 1293 Ma.

The high-grade intrusives of the c.1336 – 1293 Ma (White et al., 1999; Kirkland et al., 2008) Wankanki Supersuite and its generative event, the Mount West Orogeny, incorporate rafts of Wirku Metamorphics (Smithies et al., 2008). These intrusives are restricted to the west Musgrave Block and crop out mostly within and to the west of the Tjuni Purlka Tectonic Zone (TPTZ) (Fig. 1). Assemblages and metamorphic fabrics of this event are pervasively erased by recrystallization during the subsequent granulite facies Mesoproterozoic 1219 – 1155 Ma Musgravian Orogeny (White et al., 1999; Smithies et al., 2008).

The coincidence of two such orogenies provides a possible link through the Musgrave complex to the Albany Fraser Orogen forming a deformational belt along southern side of the West Australian Craton to Antarctica (Smithies et al., 2008; Wade et al., 2008; Evins et al., in press). Aitken & Betts (2009) question this link, suggesting that the structure is the result of a reassembly of the Mawson and Australian continents. The Musgravian orogeny is the oldest orogenic event to have affected all areas of the Musgrave block (Edgoose et al., 2004). Musgravian fabrics reflected within the Wirku Metamorphics indicate a dominant northwest-southeast structural grain (Wade et al., 2008) dominated by isoclinal and recumbent F_2 folds (Sun and Sheraton, 1992; Clarke et al., 1995). The syn- to post-tectonic granitic intrusions of the Pitjantjatjara Supersuite have all been metamorphosed to granulite facies (Smithies et al., 2008) and are divided into two distinct age groups. The c. 1219 – 1200 Ma and c. 1190 – 1155 Ma populations define the Early and Late Musgravian Orogeny respectively. Granites from this suite are geochemically separate from the Wankanki Supersuite granites, reflect A type compositional characteristics and are coeval with the voluminous A type granite suites of Laurentia (Wade et al. 2008).

Further granulite facies metamorphism imposed upon the already high-grade terrain followed, with the multiple stage c. 1075 Ma Giles event (Sun et al., 1996). The Giles Event is

considered part of the Warakurna Supersuite, which crops out over much of central and western Australia (Wingate et al., 2004). This supersuite comprises all the necessary rock representatives to be interpreted as relating to a mantle plume event (Evins et al., in press). Reassessment of the Warakurna Supersuite within the Musgrave Block has led to the new interpretation of a long lived failed rift setting, termed the Ngaanyatjarra Rift, which was active over a period of at least 50 m.y. (Evins et al., 2009). At least ten magmatic pulses are accompanied by intense deformation. They are separated with hiati of up to 10 m.y. and intrude and uncomformably overlie the > 1180 Ma Musgrave Block. Evins et al. (in press) separates this rift into a series of phases, first of which involves the deposition of basal conglomerates and sandstones followed by basalt flows. Collectively, these are termed the Kunmanarra Group. Phase 2 follows, with the intrusion of giant layered mafic-ultramafic sills at shallow depth. These first two phases occurred at times between c. 1120 and 1078 Ma. At c. 1075 Ma, Phase 3 is characterised by macroscopic folding and mafic/felsic magmatism along shear zones parallel to the previously mentioned TPTZ. By c. 1073 Ma., the Phase 2 layered mafic intrusions were exposed, allowing the extrusives of the Tollu group (Phase 9) to unconformably overlie them (Coleman, 2009). Mafic magmatism of note includes the Alcurra Suite, which hosts world class orthomagmatic Ni-Cu mineralisation (Howard et al., in press). Deformation during Phase 3 reached temperatures of up to 700-750^{o}C and pressures of 5 -11 kbar (Clarke et al., 1995). Phase 4 represents abrupt cessation of deformation and emplacement of mafic and felsic plutons. Phases 5 to 8 are each represented by a felsic pulse and separated by c. 10 Ma until c.1040 Ma.

Subsequent to the Ngaanyatjarra Rift and prior to the onset of the Petermann Orogeny, activity within the Musgrave Block was reduced to the intrusion of minor mafic and felsic rocks. Two suites of mafic dykes yield ages of c. 1000 Ma and c. 800 Ma (Sun & Sheraton, 1992; Sun et al., 1996). Two felsic dykes yield ages c. 1004 Ma and c. 622 Ma (Smithies et al., 2008).

The c. 600 Ma deposition of basement-derived sediments into the Officer Basin marks the onset of the intracratonic Petermann Orogeny (Wade et al., 2005). Deformation is

concentrated along the northern margin of the Musgrave block and was facilitated by the production of a series of major east-west trending crustal scale faults (Camacho et al., 1995; Sandiford et al., 2001) and the pervasive reactivation of pre-existing architecture (Aitken & Betts 2009). The Musgravian gneissic grain is extensively overprinted through a network of mylonite and pseudotachylite, which gradually ease to the south and east (Wade et al., 2008). The main faults include the Mann, Hinckley and the <1km thick mylonitic Woodroffe Thrust (Flottmann et al., 2004). Teleseismic interpretation by Lambeck and Burgess (1992), reveals a major offset of up to 20km in Moho depth by the Woodroffe Thrust. This thrust accommodated major north-south shortening exceeding 100km (Flottmann et al., 2004), exhuming a near full representation of crustal facies (Raimondo et al., 2009).

The structure of the Petermann Orogeny can be broadly divided into three domains, separated by some of the major faults listed above. South of the Mann fault, minor mylontic shearing and north directed kinematics feature greenschist facies metamorphism. Juxtaposed against this low-grade terrain is the hanging wall of the Woodroffe Thrust, which is the high-grade, up to 13 ± 1 kbar (Scrimgeour & Close 1999), orogenic core of the Petermann Orogeny. Mesoproterozoic gneisses and granites are considerably reworked and high strain domains display opposing kinematics (Raimondo et al., 2009). The footwall of this thrust features an abrupt lowering in metamorphic grade, which then eases to the north. Thin-skinned deformation features a series of detachment zones terminated by a back thrust zone collectively termed the Petermann nappe complex (Edgoose et al., 2004).

Despite the undeniable north directed thrust style of the Petermann Orogeny, contemporaneous mylonites in the west Musgrave Block consistenly show top to the south-west shear sense (Raimondo et al., 2009), thus bringing the kinematic evolution into question. Raimondo et al., (2009) suggest that the gravitational loading of the exhumed crust during orogenensis was enough to drive lateral crustal channel flow.

This intracontinental Petermann Orogeny, as suggested by Collins & Pisarevsky (2005),

is the likely result of far field stresses from the north - south compression of the Australian Plate during the Neoproterozoic amalgamation of Gondwana.

2.2 The metamorphic history of the Cohn Hill region

Three previous studies Clarke & Powell (1991), Kelly et al. (2006) and Werner et al. (2009) have focused on the metapelites of this region and even more studies have focussed on related gneisses to the east (White et al., 1999). Here, additional to the regional geology, are findings on the pressure and ultra–high temperature (UHT) history of the Cohn Hill region.

UHT metamorphism is typically determined within rocks of high Al and Mg content. However, these rocks are typically volumetrically rare in most metamorphic terrains (Kelsey, 2008). The exposures of Wirku Metamorphics in the Cohn Hill region stand out, as they are mainly metapelites, which are useful in determining metamorphic grade. The main metamorphic mineral assemblage from which temperatures and pressures are derived includes: garnet and sillimanite porphyroblasts mantled by a primary corona and/or symplectite of cordierite and spinel and /or a secondary cordierite and orthopyroxene corona (Fig. 9).

Clarke (1992), Clarke et al. (1995), White et al., (1999), Kelly et al., (2006) attribute migmatitic layering within the Wirku Metamorphics to the metamorphic event recently named the c.1336 – c.1293 Ma. Mount West Orogeny (D1) (Smithies et al., 2008).

Granulite facies metamorphism is inferred by White et al. (1999) to have taken place during M1. While these conditions are poorly constrained, the inference is warranted, as segregated palaeosome and leucosome domains are arranged oblique to the orientation of S2 (defined below) (Kelly et al., 2006). Additionally, given an appropriate pre M1 bulk rock composition, White et al. (2002) calculates that melting was sufficient to have caused a loss in coherence, which would have consequentially led to melt and hence water loss. Thus resulting in

an incredibly dry residue that is responsible for preserving the subsequent UHT assemblages of D2.

The respective c. 1219-1200 Ma & c. 1190 -1155 Ma Early and Late components of the Musgravian Orogeny (D2) (Smithies et al., 2008), imposed regional granulite metamorphism upon the western Musgrave Block. Clark et al. (1995) and White et al. (2002) report conditions of T = 800-850^{o}C and P = 5-6 kbar. Furthermore, the mineral assemblages at Cohn Hill yield estimated P-T conditions of approximately 7 – 8 kbar and 1000 ^{o}C with a post peak path dominated by cooling (Werner et al., 2009). Co existing D2 assemblages of spinel and quartz from Mt West also suggest temperatures < 780^{o}C (Kelly et al., 2006). These temperatures explain the existence of partial D2 palaeosome and leucosome melts.

Kelly et al. (1996) tentatively interpret c. 1300, 1200 and 1140 Ma monazite age populations from Cohn Hill as separate metamorphic events. Recent detrital and metamorphic interpretations on zircon age populations from Cohn Hill by Werner et al. (2009), support the latter two monazite ages, respectively correlating them to the Musgravian Orogeny and Ngaanyatjarra Rift. They consider c. 1300 Ma as a detrital age and assign a maximum depositional age of c. 1310 Ma for the Cohn Hill supracrustal sequence. However, textures do suggest that the monazite cores yielding this age grew during crystallisation of the leucocratic melt (Kelly et al., 2006) and it is this melting, which probably formed key anhydrous characteristics (White et al., 2002).

Most ages of Wankanki Supersuite granites fall into a range between c. 1326-1312 Ma. Strong geochemical and isotopic evidence from Wankanki Supersuite granites points towards a continental arc setting (Smithies et al., 2008). If the crystallisation age of c. 1300 Ma is correct, then these relationships provide some constraint on the deposition and burial of the protolith forming the metapelites of the Cohn Hill region.

Additional monazite ages from Cohn Hill mylonites and metapelites aim to further constrain the UHT metamorphism which is synchronous with mylonitisation. Respective ages of

1237 ± 10, 1211 ± 7and 1223 ± 15 Ma from 2 mylonites and a metapelite (Werner et al., 2009) are indicative of high grade deformation during the early Musgravian orogeny. Much of the syn- to post-Musgravian Pitjantjatarra Super Suite granites are of charnokitic composition (Smithies et al., 2008). These granites retain a primary mineralogy that suggest emplacement at extreme temperatures <1000^{o}C (Frost & Frost, 2008), which appear sufficient with extreme temperature metamorphism. On a much smaller scale, sigma and delta clasts defined by cordierite spinel intergrowths reflect the synchronous relationship of extreme temperatures to mylonitsation (Werner et al., 2009).

The corona textures as described by Clarke & Powell (1991) reflect isothermal uplift from pressures of 7-8 kbar to 4-5kbar (Werner et al., 2009). The latest age population (c. 1140 Ma) from the Kelly et al. (2006) monazite study is interpreted to represent this uplift, but is derived from an age bracket of c.1200 to 1060 Ma. As previously mentioned, Werner et al. (2009) interpret a distinct c. 1119 Ma zircon population to a metamorphic event related to the Ngaanyatjarra Rift.

3. Field Relationships

Field-work for this study involved the mapping of Cohn Hill, Minnie Hill, Red Rock and surrounding low lying outcrops (Figs. 2a & 2b). This area constitutes an overall field area of 5 x 8 km however the actual outcrop surface area is much smaller. The whole of the Cohn Hill region is classified as a partial to full exclusion zone (Werner et al., 2009) as it is of high cultural significance to the Ngaanyatjarra People. Access to Cohn Hill was restricted to its eastern face and immediately surrounding low outcrop. Low hills further south, east and west; including No Name Hill, were not mapped. Field relationships identify at least 6 key events represented by:

(1) The development of gneissic banding D1 Attributed to the Mt West Orogeny (White et al., 1999)

(2) Progressive mylonitisation and folding. D2

(3) A minor E – W oriented Mylonite

(4) Intrusion of biotite granite.

(5) Migmatisation and mylonitisation

(6) Intrusion of Pegmatitic granite

3.1 Lithology

The Cohn Hill region comprises a range of lithologies that reflect much of the deformational history of the West Musgrave Block.

3.1.1 The Wirku Metamorphics: Cohn Hill Metapelites

The Wirku Metamorphics of the Cohn Hill region are granulite facies metapelites that have undergone partial melting (D1) and subsequent segregation into palaeosome and leucosome domains (Kelly et al., 2006). Generally, the palaeosome domain retains coarse, 3-10mm diameter, garnets and ~ 2mm sillimanite crystals mantled by coronae or symplectites (Fig. 9). These mantles are typically sheared, producing sigma and delta-type kinematic indictors. Leucosomes retain smaller 2-4 mm garnet and a lot less sillimanite with minor visible symplectites or coronae. Much of the foliated matrix comprises of quartz, K-feldspar and plagioclase. Mineral lineations are defined on foliation planes by sillimanite and spinel + cordierite and also aggregates of garnet. Weathered foliation planes also yield lineations where aligned voids mark the existence of previous minerals.

Feldspar porphyroclasts form a minor, yet important, component within these metapelites. They are typically rounded and found as singular crystals up to 20mm in diameter

within all strain zones. On rare occasions, feldspar crystals form rafts up to 2m long of feldspar pophyroblasts up to 100mm in diameter (Fig. 5l). Additionally, Werner et al. (2009) interpret the ultramylonite at Ultra Mound to be of S – type granite in composition.

Outcrop scale variation within these metapelites seems to depend on a primary lithological and secondary structural control. Low strain zones preserve evidence of primary gneissic layering attributed to D1. Variations in garnet concentrations from 5% up to 35 % from layer to layer potentially illustrate the primary lithological/chemical control on the relative concentration of metamorphic minerals. The differences in concentration of these metamorphic minerals (e.g garnet) may affect the partitioning of strain during deformation. The secondary structural control is the basis on which these metapelites are mapped. Four subdivisions are created; protomylonite, low strain mylonite, mylonite and ultra-mylonite (Figs. 2a-b).

Protomylonite domains typically have well defined palaeosome and leucosomes. In the coarse grained protomylonites of Cohn Hill, garnet size is typically <6mm up to 15mm. D2 fabric (S2) begins to wrap around garnet porphyroblasts and their rotation appears limited. In a particularly low strain outcrop south of Ultra Mound, a dominance of fine grained leucosomes exists. While there are almost no garnets larger than 2mm, leucosome and mesosome domains are not extensively strung out and feature small parasitic folds with an estimated shallow southerly plunge (Fig. 5c).

The term ‘Low strain mylonite’ aims to divide the very slight and at times gradational change in S2 fabric as a purely mylonitic fabric is produced. Quartz lenses define S2 foliation wrapping around generally 10 - 4mm sized garnets. Quartz lenses are of varying lengths yet are usually up to 15mm long and 2mm wide (Fig. 5k). The ‘Mylonite’ features slightly finer grains than those of its lower strain counterpart. S2 foliation is readily defined by quartz lenses enveloping smaller 8 - 4 mm garnets. Elongate lenses vary up to 40mm and feldspar rich matrix is very fine (Figs. 8 a and b). The ‘Ultramylonite’ features strong grain size reduction and in places intense silicification of S2 fabric. Large garnets are reduced to fragments or possibly ‘rolled

down' to a maximum size of 2 -3 mm (Fig. 8c). Most importantly, within these higher strain zones, it is typically harder to see kinematic indicators defined by deformed coronae/symplectites.

Compositional variation is also represented at a larger scale with different hills retaining an overall and different **relative** signature; e.g. Cohn Hill is more felsic or less aluminous than Red Rock (Werner et al., 2009).

3.1.2 Other lithologies

Extensively boudinaged intermediate to mafic enclaves within the metapelite typically crop out from the east side of Ultra Mound to Red Rock. These enclaves are likened to the to compositionally similar enclaves within the felsic gneisses of Mt Aloysius and Mt West (Werner et al., 2009).

Three, up to 90cm wide, mafic dykes strike NNE and obliquely cut foliation on Ultra Mound, Red Rock and Minnie Hill (Fig. 2a). These dykes are tectonised yet lack foliation and are correlated to other intermediate dykes of similar orientation, which are thought to be of Pitjantjatarra Supersuite Age (Smithies, pers. comm., 2009).

The migmatite (Sample 191751) comprises of a biotite granite host injected by a porphyritic biotite granodiorite. Finally, a 200mm thick pegmatite (Sample 191763) dyke snakes across foliation on the east face of Minnie Hill. It is composed of

K-feldspar, biotite, quartz and minor magnetite.

3.2 Structure

The structures of Red Rock Map (Fig. 2a) and the smaller Cohn Hill map (Fig. 2b) are both affected by D2 which involved σ1 at an approximate south-east/north-west orientation. Consequently, they share some similarities yet retain key differences and are therefore separated in this section.

3.2.1 Red Rock Map (Fig 2a)

The pervasive gneissic foliation (S2) generally strikes NS and has a variable dip from 90 to the ~20 degrees. Ultra Mound foliations dip to the west, Red Rock foliations dip to the east and Minnie Hill foliations dip to the west again (Fig. 2a). This trend could possibly indicate the existence of larger scale D2 folds, or a series of blocks forming a type of flower structure. Centimetre to metre scale parasitic and isoclinal folds (Fig. 5 d and g) plunge either north or south up to ~ 35^{o}, indicating non-cylindrical fold hinges. These smaller scale folds may indicate the nature of the larger scale structure. Mineral lineations (L2) plunge shallowly to the north and sometimes to the south generally parallel to foliation. The large scale folding plunges very shallowly towards the south as indicated by the beta axis calculated from all poles to foliation. All good kinematic indicators along this S2 fabric indicate sinistral shear sense. The undisputed regional sinistral shear sense indicates synchronous folding/shearing or shearing after folding. Monoclinic shear fabrics on Red Rock (Fig. 2a and 2c) further reinforce sinistral shear sense of the region.

Strain levels vary from proto to ultramylonite and typically change across strike of S2 foliation. This variation is seen from the centimetre (Fig. 5e) to the kilometre scale (Fig. 3). Strain

zones mapped (Fig. 2 a-b) try to reflect the overall strain domains. Metre scale changes are common, typically low strain mylonites will hold lenses of higher strain mylonite and sometimes ultramylonite. Kilometre scale variation in strain is the observed general reduction in grain size and increase in S2 fabric within the hinges of the folds. These large overall higher strain areas (ultra and high strain mylonite) have little outcrop because of preferential weathering. Metre scale high strain zones on Red Rock and Minnie Hill illustrate this relationship with preferential weathering leaving ridges of lower strain material. However, not all higher strain zones conform to this generality. Up to two-metre wide lenses of high strain ultramylonite continue along strike at Red Rock. Grain size is particularly fine yet the matrix is highly silicic, leaving them relatively resistant to erosion.

The outcrops of Red Rock and Minnie Hill lie within the limbs the larger scale S2 folds. Within these lower strain limbs another mylonitic fabric is preserved (Fig. 3). On the peak of Red Rock, this mylonite (known as the Surfboard Mylonite) is entrained within the fabric of D2. Surfboard mylonite lineations plunge moderately to the east and kinematic indicators defined by aggregates of garnet and sillimanite indicate sinistral shear sense (Fig. 4b). Furthermore, west plunging lineations dominate the northernmost outcrops of Minnie Hill. $C^{l}S$ fabrics (which are deformed by S2) indicate a sinistral shear sense (Fig. 4c) along this plunge, indicating the presence of an east – west fabric, which was folded within S2. Further evidence of the Surfboard Mylonite is seen on the southern peak of Red Rock. The relationships here indicate that the simple entraining of S1 into S2 as seen on Red Rock's northern peak involved a folding interference pattern. Centimetre to metre scale overturned isoclinal folds are stacked upon one another. The hinges of these folds roughly plunge shallowly north/south. The lack of overprinting lineations at Minnie Hill and Red Rock suggests that this mylonite is related to the development of D2. Poor exposure inhibited a full understanding of the whole fold interference pattern.

Ultramylonite on the top of Ultra Mound (Fig. 2a), dips shallowly to the west. Lineations defined by aggregates of garnet and some very small clear yellow sillimanite plunge shallowly to

the north-west. Kinematic indicators along them indicate a dextral shear sense. This marks the surface of a later fault which cuts the regional north/south sinistral fabric. Just 20 metres to the west of the mound rest boulders of migmatite. These boulders provide evidence of the granite host being mylonitised then migmatised and vice versa (Fig. 5d-f). Chaotic folding of injection veins in the host are also noted. Additional finger-thick syn- to post-tectonic granitic veining is sheared with and cross cuts mylonitised biotite granite host and adjacent ultramylonitic metapelite (Fig. 5a-b).

This c. 20-metre wide ultramylonite/mylonite zone marks the normal contact between the Wirku Metamorphics and the migmatite. Rafts up to 2m of metapelite occur in amongst sheared migmatite, indicating a tectonic interleaving of the footwall and the hanging wall. Further south, the mapped boundary between the migmatite and metapelite fingers in towards the east and then curves off back towards the west (Fig. 2a). The migmatite within this 'finger' is un-sheared yet chaotically folded and possibly represents migmatite close to but not too far from the mylonitic contact. These relationships could mean that: (1) the mapped boundary is the naturally formed intrusive boundary of the biotite granite host or migmatite. (2) fragments from the hanging-wall, which has not eroded as fast, lie upon metapelite. (3) A wedge of migmatite has been interleaved within the footwall metapelite.

Fragmental outcrops of S2 metapelite force the boundary with the migmatite towards the west. The lack of ultramylonitic fabric (as seen on Ultra Mound) at the southern end of this boundary suggests two possibilities. Much of the sparse un sheared migmatite boulders may possibly lie on top of buried metapelite or the curvate nature represents the intrusive contact of the biotite granite.

On the east face of Minnie Hill, a small number of thin (~20cm) pegmatite dykes cross cuts the S2 foliation. This face also shows evidence of intense silicification, where a three metre wide vertical zone of mylonite appears to be siliceously altered by fluid flow. Two kilometres north of Ultra Mound (beyond the extent of Figure 2a), roadside rubble consisting of centimetre

scale mylonitic metapelite, show evidence of a similar alteration process. A large body of granite is exposed a further kilometre north.

3.2.2 Cohn Hill Map (Fig 2b)

The pervasive S2 gneissic foliation seen throughout the Red Rock map is also evident at Cohn Hill yet there remains definite variation. Cohn Hill reflects a zone of relatively lower strain, as approximately half the surface area mapped is protomylonite. Multiple metre scale isoclinal folds consistently plunge steeply towards the south, as do lineations.

Kinematics along these lineations indicates sinistral shear sense, which are typically defined by well developed coronas and symplectites (Fig. 9 a-b). Although these same kinematic indicators are evident at Red Rock, they are not as prolific as they are here. A second set of lineations (Fig. 5n), dip steeply to the west, providing opposing shear senses, many of which were unreliable. Despite the plunge of the isoclinal folding, the orientation of folding aligns with that of Red Rock. In some low strain zones, sillimanite was oriented randomly upon what seemed to be a S2 foliation. It is typically oriented parallel to transport direction in the higher strain zones of Cohn Hill, Red Rock and Minnie Hill (Fig. 5h). A small one-metre wide dextral sense mylonite (S3) cross cuts S2. Its east/west orientation and ~85^{o} dip to the south is perpendicular to the S2. Werner et al. (2009) report the arcing of a lineation upon S2 fabric, its implications are discussed in section 6.2. A pervasive late NE/SW steep cleavage is noted for the entire Cohn Hill region.

4. Optical Microstructural Analysis

The following unoriented samples were collected during the 2008 field season by M. Hand and D. Kelsey. The first three samples represent Ultra Mound, where the transition from mylonite to ultramylonite occurs over a few metres.

4.1. Sample CHR – 10 B (Fig 9a)

The outcrop from which this sample is derived hosts dextral kinematic indicators. However, in thin section it is unclear which shear sense the micro-fabric suggests. A sinistral shear sense may be supported by the following: A sigma clast is formed by quartz lenses, which trail off either end of a broken garnet. The stress on the original sigma clast resulted in a fracturing of the garnet. Shearing continued, forcing a symmetrical fabric around the two garnet fragments. If the garnet fragments were not actually part of the same original crystal, then it is quite possible that a dextral environment may have existed. Other kinematic indicators in this sample are rare. The fabric is composed of finer grains of garnet feldspar and quartz with minor Fe oxides. The lack of corona or symplectite suggests that this mylonitic fabric formed after UHT metamorphism. The reason for the opposing shear senses at different scales is probably due to the misorientation of the thin section. If a sinistral fabric was preserved, one could expect evidence of a corona or symplectite. Sinistral mylonitic microfabrics from other outcrops at Red Rock do not preserve symplectites or coronas but do hold various concentrations of sillimanite. The fabric of this sample seems to hold none.

4.2 Sample CHR - 11B (Fig 9b)

Evidence of high grade deformation is evident in this sample where thick quartz lenses show evidence of grain boundary migration (GBM) recrystallisation. A fine-grained lens of quartz and feldspar is faintly wrapped by a rolling garnet, indicating dextral shear sense, which agrees with outcrop kinematics. The mineral assemblage consists mainly of quartz feldspar and garnet, suggesting a possible granitic origin.

4.3 Sample CHR – 12 (Fig 9c)

The orientation of the ultramylonitic fabric is only just defined by a slightly coarser lateral layer of recrystallised quartz and feldspar. Kinematic indicators are non-existent while garnets are minute rolled down fragments. Almost all grains show evidence of GBM recrystallisation.

4.4 Sample CHR – 108 (Surfboard Mylonite)

This is a predominantly garnet and sillimanite mylonite with a quartz and feldspar fabric. Sillimanite up to 0.5 mm is oriented parallel to foliation. 0.5 mm diameter rolling garnets indicate dextral shear sense; this is questionable due to the unoriented nature of the original sample. Spinel and cordierite are absent. A late fracture cross cuts foliation and has allowed minor biotite alteration.

5. Geochronology

The two samples selected for geochronology represent key field relationships. Sample 191751 (Migmatite) represents a time of intense heating and localised melting. Given the high temperature history of the field area, the timing of migmatisation provides a key insight to this history. Sample 191763 (Granitic pegmatite dyke) cross cuts foliation. Its age provides a constraint on the shearing event, which from field relationships, is synchronous with extreme temperature metamorphism. A third sample interpreted as syn to post tectonic with mylonitisation at Ultra Mound was processed thoroughly, yet produced little to no zircons.

5.1 Analytical Procedure

Crushing and zircon separation took place at the Mawson Laboratories, University of Adelaide. Samples were broken into fist sized blocks and then passed through a clean jaw crusher. The resulting grit was further crushed in a tungsten carbide ring mill. Sieving simultaneously through 75 and 300 µm mesh produced a 75-300 µm fraction which was then panned. The dried pan fraction was passed over with a strong hand magnet and then run through the methylene ioidide. The heavy mineral fraction is carefully removed and dried. Approximately 70-100 zircons from each sample were hand picked with the aid of a binocular microscope.

Crystals were then mounted by GSWA laboratories according the specifications listed in Wingate & Kirkland (2009). Each sample had its own mount and several fragments of the set up grain CZ3, the primary U-Pb calibration Temora standard (BRA and BRB) and zircons of high ^{238}U and Pb concentrations (OGC) to assist mass peak setup. The mount was polished to the approximate half-width of the zircon grains. Internal zircon morphology was analyzed using a cathodoluminescence (CL) detector on a Philips XL20 scanning electron microscope (SEM)

operating at 12.0 kV, located at Adelaide Microscopy. The operating guidelines regarding the SHRIMP are detailed in Wingate & Kirkland (2009).

5.2 Sample descriptions

The internal zircon morphologies were studied with the aid of a CL detector in a SEM. Several representative samples with respective spot locations are displayed in Figs. 6 - 7. The degree of luminescence is determined by the concentration of certain trace elements (e.g. U, Hf, Y) within the zircon structure (Koschek, 1993). Low cathodoluminescence (Low CL) relates to the higher levels of U, while the opposite is true for lower U concentrations, where a high CL is produced.

5.2.1 Migmatite

The host is a mesocratic biotite granite injected by plagioclase porphyritic biotite granodiorite. The biotite granite host contains abundant apatite and zircon (Werner et al., 2009), occasional K-feldspar phenocrysts up to 1cm, and enclaves of quartz amphibolite up to 10cm.

Zircons isolated from this sample are dominantly euhedral and colourless to light pink. Grains are up to 420 mm long, with aspect ratios from 3:1 up to 5:1. Cathodoluminescence (CL) images reveal variable emission but generally display strongly resorbed cores. Distinct rim overgrowths and the lobate margins between domains within the same crystal indicate some magmatic resorption process. A CL image of representative zircons is shown in Fig. 7.

5.2.2 Pegmatite Dyke

This is a K-feldspar granite pegmatite which cross cuts S2. No thin section was made of this sample. The visually estimated mineralogy includes 35 % quartz, 40 % orthoclase, 15 % plagioclase and 10 % biotite. The K-feldspar occurs as crystals up to 45 mm long with less abundant phenocrysts of plagioclase up to 15 mm long. Quartz crystals are up to 15mm long. Biotite, up to 5 mm long is disseminated throughout. Zircons isolated from this sample reflect

two morphologies; xenocrystic and pegmatitic. The xenocrystic zircons display rounded rims, are dominantly colourless and short. Grains are up to 150 mm long, with some aspect ratios up to 4:1. CL images reveal variable emission but generally display idiomorphic zoning. Their lack of euhedral faces and smaller size then that of the pegmatitic zircons potentially indicates an inherited origin (Fig 6 c-d). Rim overgrowths are present only within the xenocrystic zircons and potentially indicate some resorption process. A CL image of representative zircons is shown in Figure 6. The pegmatitic zircons are large, euhedral and light brown (Fig 6 a-b). Grains are up to 650 mm long with aspect ratios usually 2-3:1, but sometimes higher. CL images reveal relatively homogenous low emission and no rim overgrowths. One to two domains exist within these crystals.

5.3 Analytical details

The two samples were analysed on the 11th and 12th of September 2009, using SHRIMP-B at Curtin University of Technology. The effects of common lead were minimized by rastering the analysis site for two minutes before analysis.

5.3.1Migmatite

This sample was analysed over two sessions. Analyses 1.1 to 11.1 (spot numbers 1–13 inclusive) were obtained during the first session, together with 5 analyses of the BRB standard that indicated an external spot-to-spot (reproducibility) uncertainty of 1.69% (1s), and a $^{238}U/^{206}Pb^{*}$(radiogenic lead) calibration uncertainty of 0.75% (1s). Analyses 12.1 to 18.2 (spot numbers 14–23 inclusive) were obtained during the second session, together with another five analyses of the BRB standard which indicated an external spot-to-spot (reproducibility) uncertainty of 0.45% (1s), and a $^{238}U/^{206}Pb^{*}$ calibration uncertainty of 0.95% (1s). Calibration uncertainties are included in the

errors of $^{238}U/^{206}Pb^*$ ratios and dates listed in Table 1. Common-Pb corrections were applied to all analyses using contemporaneous common-Pb isotopic compositions determined according to the Pb isotopic model of Stacey and Kramers (1975), and these data are presented in Figure 2 and Table 1.

5.3.2 Granitic Pegmatite Dyke

Analyses 1.1 to 17.1 (spot numbers 1–17 inclusive) were obtained together with 7 analyses of the BRB standard that indicated an external spot-to-spot (reproducibility) uncertainty of 0.88% (1s), and a $^{238}U/^{206}Pb^*$ calibration uncertainty of 0.37% (1s). Calibration uncertainties are included in the errors of $^{238}U/^{206}Pb^*$ ratios and dates listed in Table 1. Common-Pb corrections were applied to all analyses using contemporaneous common-Pb isotopic compositions determined according to the Pb isotopic model of Stacey and Kramers (1975), and these data are presented in Figure 2 and Table 1.

5.4 Results and Interpretation

SHRIMP U–Pb zircon data are reduced using the excel add ins SQUID 2.23 and Isoplot 3.67 with decay constants as recommended by Steiger and Jäger (1977).

5.4.1 Migmatite

Twenty three analyses were obtained from 18 zircons. Results are listed in Table 1, and shown in a concordia diagram (Fig. 8c). All but three analyses are concordant and define two coherent groups based on $^{207}Pb/^{206}Pb$ and Th/U ratios. Group I comprises 10 analyses from an original 13 (Table 1), which yield a concordia age of 1160 ± 15 Ma (MSWD = 1.6) (Fig. 8a). These analyses have moderate Th/U ratios (1.20–0.09) and were located on zircon cores, which in most cases had

been somewhat resorbed (Fig 1). Their ages spread somewhat towards the age of Group M. This spread is interpreted as a loss of radiogenic ^{206}Pb from the magmatic population (Fig 8b-c) (possibly due to the event assigned by Group M). Group I is interpreted to represent the age of magmatic crystallisation of the biotite granite host. Group M comprises 8 analyses (Table 1), which yield a concordia age of 1066 ± 5 Ma (MSWD = 0.77) (Fig. 8b). These analyses have low Th/U ratios (0.04–0.36) and were located on homogenous and euhedral zircon rims (Fig. 7). The date of 1066.0 ± 5.0 Ma for 8 analyses in Group M (Fig. 8a) is interpreted as the age of a high grade metamorphic event.

5.4.2 Granite Pegmatite dyke

Eighteen analyses were obtained from 17 zircons. All but two analyses are concordant based on $^{207}Pb/^{206}Pb$ ratios. Group I comprises 16 analyses (Table 1), which yield a concordia age of 1135 ± 5.9 Ma (MSWD = 1.9). These analyses have variable Th/U ratios (2.16–0.32) and were located on zircons whose morphologies were both xenocrystic and pegmatitic. Despite there being two visually distinct populations of zircon. The potentially inherited grains may have been reset in the magmatic event involving the crystallisation of the pegmatoidal population. The date of 1135 ± 5.9 Ma for 16 analyses in Group I is interpreted as the age of magmatic crystallization of the granitic pegmatite dyke and its source emplacement.

6. Discussion

6.1 Timing of Events

Faded oscillatory cored zircon populations from the Cohn Hill region indicate Musgravian metamorphism effective between c. 1229 and c. 1181Ma and a second event at c. 1119 Ma related to the Ngaanyatjarra Rift (Werner et al., 2009). Monazite age populations from Kelly et al. (2006) are reported at c. 1300, 1200 and 1140 Ma. Werner et al. (2006) correlate the last two monazite populations with their two zircon populations, respectively. Four more monazite ages from the Cohn Hill region yield ages spread between c. 1211 – 1237 Ma (Werner et al., 2009). Field relationships indicate that D2 is synchronous with extreme temperature metamorphism, which as explained in section 2.1, is coincident with the Musgravian Orogeny. The synchronicity of ultra high temperature metamorphism and mylonitisation suggests that decompression occurred during D2. However, these synchronous relationships do not exist everywhere. From field observations the higher strain zones within the hinges of the large scale folds typically do not retain the decompressional assemblages seen on Cohn Hill and have suffered variable degrees of grain size reduction.

This suggests that D2 involved the development of kilometer scale open folds, progressive shearing and possibly isothermal decompression. Within areas of low strain, relatively undeformed coronae and symplectites remain, yet they still lie within S2. The Corona textures as described by Clarke & Powell (1991) reflect isothermal uplift from pressures of 7-8 kbar to 4-5kbar. D2 seems to have assisted this transition.

The beginning of D2 is marked by the distinct Musgravian zircon and monazite ages as listed at the beginning of the section. The oldest D2 fabric, the 'Surfboard Mylonite', has the oldest monazite age of c. 1237 Ma (Werner et al., 2009). Additionally, metamorphic rims from Cohn Hill zircons yield an age population spread from c. 1229 – 1181 Ma (Werner et al., 2009). This provides a good upper constraint and suggests metamorphism before and during the Early and Late Musgravian Orogeny. Kelly et al. (2006) concludes that isothermal decompression occurred after c. 1200 Ma.

The crystallization age of the pegmatite dyke (191763) at c. 1135 ± 5.9 Ma constrains D2 to between c. 1237 – 1135 Ma. Kelly et al., (2006) report monazite ages purely from the mesosome domain, which yield a similiar age of c. 1135 Ma. The authors associate this age with the event responsible for garnet retrogressing to secondary biotite (Kelly et al., 2006) This agrees with microscopic (Fig. 10a) and field observations of fluid alteration in the vicinity of granite emplacement. The constraint that this pegmatite provides on the timing of D2 means that later deformation (i.e. emplacement of Giles Intrusions) was not responsible for the decompressional textures observed by Clarke & Powell (1991). Therefore any further isothermal decompression must have either already happened or was a result of this event. This implies that the various lower P post peak assemblages seen in the Wirku Metamorphics of the West Musgrave Block (White et al., 2002; Clarke & Powell, 1991), reflect the evolution of the Musgravian Orogeny (Wade et al., 2008).

Interestingly, the age of this pegmatite falls outside the emplacement age of Late Musgravian granites as assigned by Smithies et al. (2008). However, these definitions are based on granites from the BATES region in the eastern West Musgrave Block, further geochronology of granites to the west may suggest a wider bracket for Late Musgravian granites. Edgoose et al. (2004) assign the emplacement of the Pitjantjatjara Supersuite at a wider age range of c. 1190 – 1120 Ma. Considering this, the pegmatite may be a late addition to this suite of Musgravian granite.

As previously mentioned, Werner et al. (2009) correlate the c. 1140 Ma monazite population with their distinct zircon population of c. 1119 Ma and attribute it to the onset of the event known as the Ngaanyatjarra Rift. This monazite population is of high error (earliest age is c. 999Ma) and Kelly et al. (2006) suggest a most probable mix of multiple populations. Furthermore, the age gap between the granite and the onset of the Rift is only c. 15 m.y, which may suggest a more complex transition from the late Musgravian orogeny towards the onset of the Ngaanyatjara Rift.

The migmatite (191751) yielded two ages. Zircon cores reveal a magmatic crystalisation age of the biotite granite host at 1160 ± 15 Ma and rims indicate migmatisation at 1066 ± 5 Ma. The biotite granite falls within range of the compositional variety of Pitjantjatjara Supersuite granites as suggested by Edgoose et al. (2004). However, it is not representative of the high grade charnokites and rapakivi granites which are so popularly reported in the Pitjantjatjara Supersuite of the West Musgrave Block. The migmatite host lacks a granoblastic texture (Werner et al., 2009) and granulite indicator minerals, which suggests emplacement at a relatively lower grade than the granulite facies metapelites. Edgoose et al., (2004) describes a possibly correlative biotite granite of the Mantarurr Suite just north of the Woodroffe Thrust, which is surprisingly similar in composition, morphology and age. The emplacement of the sampled biotite granite is attributed to the series of magmatic events defining the late Musgravian Orogeny.

The emplacement age of the biotite granite could be used to place a constraint on D2 if the boundary separating the two is interpreted as a true intrusive contact. Its curvate nature seems to suggest that this is the case, however these curves are derived from mapping scree, which is not totally reliable (as opposed to the reliable dyke). Nevertheless, it is possible that isothermal decompression may have occurred prior to or during c. 1160 Ma.

Field relationships suggest that normal dextral faulting was activated during migmatisation of the biotite granite rather than during/after granite emplacement (section 3.3.1). Nevertheless, field relationships allow one to say that the fault was active at a time before migmatisation and after granite emplacement.

As previously mentioned, there remains strong evidence for deformation during migmatisation (Sections 3.3.1; 4.2 and Figs a-b, d-e). The high temperature grain boundary migration recrystalisation of the ultramylonite in the zone points to a high temperature shearing event. The age of 1066 ± 5 Ma is interpreted as the age of migmatisation and considerable deformation. A series of granitic veins, syn to post c. 1066 tectonism, cross cut the mylonitic fabric of the metapelite immediately adjacent to the fault. It is possible that the veins represent a later minor local melt and if this is the case, indicate reactivation of this boundary. The intense grain size reduction of the associated ultramylonite suggests that reactivation was quite possible.

However, if these veins are interpreted as part of the migmatisation event, then they effectively stitch the current positioning of the foot wall and hanging wall at c. 1066 Ma.

The wide spread of monazite ages which constitute the c. 1140 Ma monazite population (Kelly et al., 2006), include a series of earlier ages, which probably record the high temperature conditions during the c. 1075 Ma Giles Event. Any further relation between these monazite ages and migmatisation is weak.

Evins et al. (in press) explains how the Ngaanyatjarra Rift is expressed in the west Musgrave complex as a intricate series of events, occurring over a time span of at least 50 m.y. The deformation associated with migmatisation may be related to Phase 3 of this rift, which is characterized by mafic to felsic magmatism associated along coeval linear shear zones (Evins et al., in press). This adds further suggestion to the fault activation during migmatisation.

Interestingly, the age of migmatisation also correlates with the age of Ni-Cu and Cu mineralized gabbros dated at c.1068 Ma and c. 1067 Ma (Howard et al., in press), respectively. Howard et al. (in press) interpret these events as synchronous with the Alcurra dyke suite. The implications of this upon the Cohn Hill region are discussed in section 6.3.

6.2 Strain partitioning

As previously mentioned, field relationships identify at least 6 deformational periods which are key to the understanding of the structural evolution of the Cohn Hill Supracrustal sequence. Some of these key relationships are typically preserved within zones of relatively low strain. Therefore, an understanding of how strain is partitioned within shear zones becomes of high importance.

At high crustal temperatures, the rheological difference between adjacent rocks diminishes and shear zones are typically wider (Passchier & Trouw, 2005). The partially melted gneisses and mylonitic fabrics of the Cohn Hill area reflect this relationship and hence preserve a kilometre scale shear zone. While there is evidence of other deformation, it is the dominant D2 sinistral shear zone, which holds the key to previous fabrics. S2 and L2 imply a SE/NW shortening direction. Within this shear zone, strain varies across strike at the micro to kilometre scale, creating a variety of fabrics from proto to ultramylonite. It is reported that quite different structural fabrics can develop in different rock types within a single deformational event (Pereira & Silva, 2004). This variation can be explained in terms of simultaneous pure and simple shear, which results in the gradual partitioning of strain into coaxial and non coaxial components (Fossen & Tikoff, 1993, 1998). Typically, higher strains result in non-coaxial deformation and lower strains produce coaxial deformation. A gradational range of deformational modes, lie in between the low and high strain end members (Fossen & Tikoff, 1993).

On comparison of Figures 2 a(Red Rock) b(Cohn Hill), 3 and field relationships, a number of differences/similarities are of note, and are summarized in the following points:

- They (Red Rock and Cohn Hill) both have a similar foliation associated with D2
- Both display isoclinal folds with lineations generally parallel to their hinges
- Both indicate sinistral shear sense for D2.

- Both preserve earlier evidence of shearing
- Cohn Hill folds plunge steeply to the south while Red Rock folds plunge very shallowly to the south.
- Red Rock outcrops are of a generally higher strain than those of Cohn Hill.
- High strain zones are focussed within the hinges of large scale folds.

The similarities suggest that the relatively low strain zones of Red Rock and Minnie Hill, and the protomylonite of Cohn Hill have variably preserved evidence of a previous E/W trending mylonite. Cohn Hill expresses this mylonite with cross cutting lineations and multiple kinematic indicators while Red Rock preserves the folding interference pattern and the original mylonitic fabric. Minnie Hill preserves a general transition of lineations from north to west.

However, the differences that remain suggest the Red Rock area was dominated by simple shear and generated a well developed sinistral fabric parallel to the bulk shearing direction. This is substantiated by the development of metre scale monoclinic fabrics (Fig 2c). Alternatively, the lower strain of Cohn Hill may have been influenced by pure shear, which involved a component of extension orthogonal to SE/NW shortening direction. It reality both parts of the shear zone probably experienced extension in the vertical component yet there still remains a relative difference of note. This variation in shear styles explains the variation in the plunge of isoclinal folds which are generally parallel to L2. The reason for this variation in strain may be related to the nature of the walls of the shear zone or possibly due to an overall bulk difference in composition. Cohn Hill is considered more felsic than Red Rock (Werner et al., 2009) and retains a substantially larger amount of large garnets. It may be possible that a more crystalline Cohn Hill was ‘squashed’ while a finer grained Red Rock, was ‘stretched’, developing a more intense fabric. Akin to a porphyroclast in a mylonitic fabric. Werner et al. (2009) report the arching of a series of lineations upon the gneissosity surface and therefore question the validity of lineations in that area. The previously used analogy of a porphyroclast may be able to explain this. The movement of individual crystals across the face of the ‘porphyroclast’ may experience localised

forces much like an eddy, which could force an arching of general lineation orientation. Furthermore, the bands of various strain metapelite vary in garnet concentration from close to nothing to up to ~40%. These differences in concentration occur over the metre scale. The evidence of partial melting during D2 (Kelly et al., 2006) provides a possible reason for this segregation as deformation is likely to cause strain partitioning between molten and solid phases. Hence resulting in a segregation of the more viscous phase (Vigneresse et al., 1999).

6.3 Structural evolution of the Cohn Hill supracrustal sequence.

As previously noted, the S2 preserves evidence of an earlier E/W trending 'Surfboard mylonite'. Evidence of this mylonite on Red Rock, Cohn Hill and Minnie hill suggest that it was a relatively widespread (kilometre scale) sequence of deformation. Interference fold patterns suggest that this E/W mylonite was prior to D2 .The relative simple 'stacking' of folds, may indicate that it was not affected by a prior phase of deformation apart from its derivative. It is possible that the Surfboard Mylonite represents a detachment shear zone. It may be interpreted as either compressional or extensional, but if related to D2, may represent the beginnings of a compressional system. This system would see the relative movement of the upper plate from west to east, followed by collision and the arrangement of upright, tight, north-south striking folds. Gradual reorientation of $\sigma 1$ from east-west to southeast-northwest sees the onset of a transpressional, sinsitral shear zone.

This model is generally in agreement with the model of Aitken & Betts (2009), who suggest that The Musgravian Orogeny, involved a primary shortening direction which was oriented northwest – southeast. Tectonothermal events possibly during or after the late Musgravian Orogeny yet no later that c. 1135 Ma, resulted in the isothermal uplift of the metapelites from ~ 8 – 4kb (Clarke &

Powell, 1991). The c. 1160 & 1135 Ma crystallisation ages of granites sampled are both younger than the latest Pitjantjatarra granite from the BATES region. This suggests that magmatism may young towards the west of the Musgrave Block.

At a time between c.1120 to 1078 Ma, roof uplift is suggested to have occured to accommodate the emplacement of Phase 2 Ultramafic sills (Evins et al., in press). This is followed by c. 1066 Ma syntectonic migmatisation, that probably saw the activation and further relative uplift of the Cohn Hill metapelite. A thin, steep E/W dextral mylonite (Fig. 5j) cuts Cohn Hill and may have accommodated this dextral extension. A late, predominantly steep NE dipping pervasive cleavage may represent all that is evident of this event or it could relate to Petermann aged deformation.

6.4 Exploration Significance

The age of migmatisation at 1066 ± 5 Ma is coincident with the (Seat, 2008) 1068 ± 4 Ma orthomagamtic Ni-Cu Mineralisation of Nebo Babel and the (Howard et al., in press) 1067 ± 8 Cu mineralized gabbros north of Jameson. Howard et al. (in press) stress that these identical ages of mineralization indicate a pulse of highly prospective magmatism. The migmatite near Ultra Mound suggests that migmatisation was associated with the lit par lit injection of granodiorite (Werner et al., 2009). However, just a few kilometers west of Cohn Hill is a chrysoprase mine, which suggests the presence of an ultramafic intrusion. If the migmatisation involved the synchronous emplacement this ultramafic body, then the region immediately to the west of Ultra Mound is a potential host of orthomagmatic mineralization.

Additionally, The fault marking the migmatite zone trends northwards towards Jameson Range. The timing of this fault is strongly linked to the time of migmatisation and could indicate a ~30km lineament along which mineralization may have occurred.

7. Conclusions

Key field relationships combined with U-Pb SHRIMP geochronology have allowed for a deeper understanding on the evolution of the Wirku Metamorphics of the West Musgrave Block and especially the Cohn Hill the supracrustal sequence.

Six main conclusions are made:

(1) The U-Pb SHRIMP crystallisation age of 1135 ± 5.9 from a pegmatite dyke confirms the retrograde event suggested by Kelly et al., (2006). Decompression from pressures of ~7 kbar to ~4kbar (Clarke & Powell) is constrained to within the limits of the Musgravian orogeny and is not related to Giles aged events.

(2) Simultaneous UHT conditions and sinistral, transpressive shearing assisted decompression yet the shearing extent and its timing is unclear. All that is known is that its fabric is cut by the c. 1135 intrusion

(3) Relatively low strain zones from the same shearing event preserve evidence of an earlier fabric, which can assist in understanding the tectonic development of the Musgravian Orogeny.

(4) The U-Pb SHRIMP core age of 1160 ± Ma represents the crystallization age of a biotite granite which may be very tentatively used to further constrain the timing isothermal decompression. Stronger field relationships are needed to confirm this constraint.

(5) The U-Pb SHRIMP rim age of 1066 ± 5 Ma is the age of migmatisation and probable initiation of a high temperature mylonitic normal fault. These events represent tectonothermal activity during Phase 3 of the Ngaanyatjarra Rift (Evins et al., in press).

(6) The 1066 ± 5 Ma, migmatistion age is coincident with significant mineralization associated with the Alcurra dyke suite (Howard et al., in press). Structural relationships and field observations suggest a possible setting for orthomagmatic mineralization to the west of Cohn Hill.

8. Acknowledgements

I thank my supervisor Alan Collins, as well as Dave Kelsey and Martin Hand for their help throughout the year. Many thanks go to Hugh Smithies, Heather Howard, Chris Kirkland, Mario Holmes, Michael Wingate, Mario Werner and of course Brian Moore for all the amazing GSWA support. I also thank my buddy, Pete Coleman, who helped me get in and out of a number of sticky situations.

9. References

Aitken, A. R. A. & and Betts, P. G. 2009. Constraints on the Proterozoic supercontinent cycle from the structural evolution of the south-central Musgrave Province, central Australia. Precambrian Research 168, 284 – 300.

Camacho, A. & Fanning, C. M. 1995. Some isotopic constraints on the evolution of the granulite and upper amphibolite facies terranes in the eastern Musgrave Block, central Australia. Precambrian Research 71, 155-181.

Camacho, A., Vernon, R. H. & Fitzgerald, J. D. 1995. Large volumes of pseudotachylite in the Woodroffe Thrust, eastern Musgrave Ranges, Australia. Journal of Structural Geology 17, 371-383.

Clarke, G.L., Powell, R., 1991.Decompressional coronas and symplectites in granulites of the Musgrave Complex, Central Australia. Journal of Metamorphic Geology 9 (4), 441–450.

Clarke, G. L., Buick, I. S., Glikson, A. Y. & Stewart, A. J., 1995. Structural and pressure–temperature evolution of host rocks of the Giles Complex, western Musgrave Block, central Australia. AGSO Journal of Australian Geology and Geophysics, 16, 127–146.

Collins, A. S. & Pisarevsky, S. A. 2005. Amalgamating eastern Gondwana: The evolution of the Circum-Indian Orogens. Earth Science Reviews 71, 229-270.

Edgoose, C.J., Scrimgeour, I.R., and Close, D.F., 2004, Geology of the Musgrave Block, Northern Territory: Northern Territory Geological Survey Report 15, 44 p.

Evins, PM, Smithies, RH, Howard, HM and Kirkland, CL in press, Devil in the detail; the 1150 – 1000 Ma magmatic and structural evolution of the Ngaanyatjarra Rift, west Musgrave Province, Central Australia: Precambrian Research.

Flöttmann, T., Hand, M., Close, D., Edgoose, C.J., and Scrimgeour, I.R., 2004, Thrust tectonic styles of the intracratonic Alice Springs and Petermann orogenies, central Australia, in McClay, K.R., ed., Thrust Tectonics and Hydrocarbon Systems: American Association of Petroleum Geologists (AAPG) Memoir 82, p. 538–557.

Fossen, H. & Tikoff, B. 1993. The deformation matrix for simultaneous simple shearing, pure shearing and volume change, and its application to transpression-transtension tectonics. Journal of Structural Geology 15(3-5), 413-422

Frost, BR, and Frost, CD, 2008, On Charnockites: Gondwana Research,13, 30–44.

Glikson, AY, Stewart, AT, Ballhaus, GL, Clarke, GL, Feeken, EHT, Level, JH, Sheraton, JW and Sun, S-S 1996, Geology of the western Musgrave Block, central Australia, with reference to the mafic–ultramafic Giles Complex: Australian Geological Survey Organisation (Geoscience Australia), Bulletin 239, 206p

Howard, HM, Smithies, RH, Kirkland, CL, Evins, PM and Wingate, MTD, (in press), Age and geochemistry of the Alcurra suite in the west Musgrave Province and implication for orthomagmatic Ni – Cu – PGE mineralization during the Giles Event.

Kelly, N.M., Clarke, G.L., Harley, S.L., 2006.Monazite behaviour and age significance in poly-metamorphic high-grade terrains:Acase study fromthewestern Musgrave Block, central Australia. Lithos 88 (1–4), 100–134.

Kelsey, D. E., 2008. On ultrahigh-temperature crustal metamorphism. Gondwana Research. 13, 1-29.

Kirkland, CL, Wingate, MTD, and Bodorkos, S, 2008a, 183496: Geochronological dataset 747, in Compilation of geochronological data: Geological Survey of Western Australia.

Koschek, G., 1993. Origin and significance of the SEM cathodoluminescence from zircon. Journal of Microscopy, 171, 223-232.

Lambeck, K. & Burgess, G. 1992. Deep crustal structure of the Musgrave Block, central Australia: results from teleseismic travel-time anomalies. Australian Journal of Earth Sciences 39, 1-20.

Maboko, M. A. H., McDougall, I., Zeitler, P. K. & Williams, I. S. 1992. Geochronological evidence for ~530- 550 Ma juxtaposition of two Proterozoic metamorphic terranes in the Musgrave Ranges, central Australia. Australian Journal of Earth Sciences 39, 457-471.

Passchier, C.W. and Trouw, R.A.J., 2005. Microtectonics. Springer, Berlin, 289 pp.

Pereira, M. F. & Silva, J. B. 2004. Development of local orthorhombic fabrics within a simple-shear dominated sinistral transpression zone: the Arronches sheared gneisses (Iberian Massif, Portugal). In: Flow Processes in Faults and Shear Zones (edited by Alsop, G. I., Holdsworth, R. E., McCaffrey, K. J. W. & Hand, M.) Geological Society of London, Special Publications 224, 215-227.

Raimondo, T., Collins, A. S., Hand, M., Walker-Hallam, A., Smithies, R. H., Evins, P. M., Howard, H. M., 2009. Ediacaran intracontinental channel flow. Geology. p. 291- 294

Sandiford, M., Hand, M. & McLaren, S. 2001. Tectonic feedback, intraplate orogeny and the geochemical structure of the crust: a central Australian perspective. In: Continental reactivation and reworking. (edited by Miller, J. A., Holdsworth, R. E., Buick, I. S. & Hand, M.). Geological Society of London, Special Publications 184, 219-236.

Scrimgeour, I.R., and Close, D., 1999, Regional highpressure metamorphism during intra cratonic deformation: The Petermann orogeny, central Australia: Journal of Metamorphic Geology, v. 17, p. 557–572.

Seat, Z 2008, Geology, petrology, mineral and whole-rock chemistry, stable and radiogenic isotope systematics and Ni–Cu–PGE mineralization of the Nebo–Babel Intrusion, west Musgrave, Western Australia: University of Western Australia, PhD thesis (unpublished), 237p.

Smithies, RH, Howard, HM, Evins, PM, Kirkland, CL, Bodorkos, S and Wingate, MTD 2009a, The west Musgrave Complex — new geological insights from recent mapping, geochronology, and geochemical studies: Geological Survey of Western Australia, Record 2008/19, 20p.

Stacey, JS and Kramers, JD 1975, Approximation of terrestrial lead isotope evolution by a two-stage model: Earth and Planetary Science Letters, v. 26, p. 207–221.

Steiger, RH and Jäger, E 1977, Subcommission on geochronology: convention on the use of decay constants in geo- and cosmochronology: Earth and Planetary Science Letters, v. 36, p. 359–362.

Sun, S.-S. & Sheraton, J., 1992. Zircon U/Pb chronology, tectonothermal and crust forming events in the Tomkinson Ranges, Musgrave Block, central Australia. Australian Geological Survey Organization, Research Newsletter, 17, 9–10.

Sun, S.-S., Sheraton, J. W., Glikson, A. Y. & Stewart, A. J., 1996. A major magmatic event during 1050–1080 Ma in central Australia and an emplacement age for the Giles Complex. AGSO Research Newsletter, 17, 9–10.

Vigneresse, J. L., Tikoff, B. 1999. Strain partitioning during partial melting and crystallizing felsic magmas. Tectonophysics 312, 117 – 132.

Wade, B. P., Hand, M. & Barovich, K. M. 2005. Nd isotopic and geochemical constraints on provenance of sedimentary rocks in the eastern Officer Basin, Australia: implications for the duration of the intracratonicPetermann Orogeny. Journal of the Geological Society of London 162, 513-530.

Wade, B. P., Kelsey, D.E., Hand, M. & Barovich, K. M. 2008. The Musgrave Province: Stitching north, west and south Australia. Precambrian research 166, 370-386.

Werner, M, Smithies, RH, Howard, HM, Evins, PM, Kelsey, D, Hand, M, Maier, W 2009,. West Musgrave Province: GSWA Field Excursion 2009. Geological Survey of Western Australia, 69p.

White, R.W., Clarke, G.L., Nelson, D.R., 1999. Shrimp U–Pb zircon dating of Grenville-age events in the western part of the Musgrave Block, central Australia. J. Metamorph. Geol. 17, 465– 481.

White, R.W., Powell, R., Clarke, G.L., 2002. The interpretation of reaction textures in Fe-rich metapelitic granulites of the Musgrave Block, central Australia: constraints from mineral equilibria calculations in the system K2O–FeO–MgO–Al2O3–SiO2–H2O–TiO2–Fe2O3. Journal of Metamorphic Geology 20 (1), 41–55.

Wingate, MTD & Kirkland, CL 2009. Introduction to geochronology information released in 2009: Geological Survey of Western Australia, 5p.

Wingate, MTD, Pirajno, F and Morris, PA 2004, Warakurna large igneous province: a new Mesoproterozoic large igneous province in west-central Australia: Geology, v. 32, p. 105–108.

Figure Captions

Figure 1. Regional geological map of the Musgrave block; illustrating its position relative to the Amadeus and Officer Basins. The inset map highlights the Cohn Hill region and outcrop which was mapped in this study. Modified after Raimondo T. 2006.

Figure 2. *(a)* Geological strain map of Red Rock and surroundings illustrating the variance in strain and the macro-scale sinistral fabric developed during D2 mylontisation. Stereoplots of foliations reveal several limbs to larger scale folding plunging shallowly to the south. This folding overprints the E/W sinistral 'Surfboard' mylonite. Lineations dip shallowly to the north and south however vary where previous fabrics are preserved and where strain regimes change. Folding is interpreted to be syn-D2 mylontisation. Also shown is the contact between D2 mylonite and Migmatite and SHRIMP monazite and zircon ages*;(b)* Geological strain map of the East face of Cohn hill. Isoclinal folds dip steeply to the south. Lineations orient parallel to fold plunge as well as steeply north and west. Strain is lower overall in this area*;(c) Inset in 2a*. Metre-sale CS fabric developed within mylonite on Red rock reflecting the sinistral shear sense of the D2 mylonite.

Figure 3. Schematic cross section from A to A'. Relatively low and high strain zones correspond to the limbs and hinges respectively. Younger 'Surfboard Mylonite' is preserved within a lower strain lens. The migmatite/mylonite contact illustrates the juxtaposed granulite facies gneiss against the presumably lower amphibolite facies migmatite through a normal fault, which has experienced at least two stages of reactivation.

Figure 4. Key kinematic features of mylonite from various outcrops within Fig. 2(a): *(a)* Red Rock mylonite. A spinel/cordierite symplectite trails off a 1cm garnet producing a delta clast revealing sinistral shear sense*; (b)* Spinel/cordierite symplectites trail off garnets with the surfboard mylonite producing sinistral delta and sigma clasts (top of Red Rock)*; (c)* Preserved C' – type shear band formation in silicic lens within Surfboard Mylonite revealing sinistral shear sense (north of Minnie Hill). Overprinting by D2 folding/shearing distorts shear band *;(d)* Foliation around a virtually non existent feldspar porphyroblast reveals a sigma shape and sinistral shear sense (Minnie Hill).

Figure 5. Various key field relationships, pen for scale: *(a)* Rare, centimetre thick granitic veins cross cut D2 mylonitic foliation, close to migmatite boundary*;(b)* Visually and texturally similar to previously mentioned granitic veins cut mylonitic foliation within biotite granite (migmatite host)*;(c)* Parasitic folding within low strain gneiss*;(d)* Sheared Migmatite*;(e)* Grain size variation and reduction within ultra-mylonite. 1mm garnets dissipate until non-existent, matrix becomes very siliceous*;(f)* Un-sheared chaotically folded injection migmatite possibly tectonically interleaved within the footwall mylonitic gneiss*;(g)* Isoclinal folding dipping moderately towards north with lineations following suit (1km South of Ultra Mound)*;(h)* Aggregates of spinel and sillimanite defining mineral lineations (North Peak, Minnie Hill)*;(i)* Surfboard mylonite (D1) being folded into D2 mylonite (North Peak, Red Rock)*;(j)* Later stage (D3) mylonite shearing D2 protomylonite. Dextral shear sense. Hammer for scale. (Cohn Hill); (k)Example of low strain mylonitic fabric (Red Rock);(l) Example of high strain mylonitic fabric (Red Rock);(m)Sheared raft of megacrystic granite (Minnie Hill);(n) Overprinted lineations (Cohn Hill).

Figure 6. Cathodoluminescence image of representative zircons from sample 191763: Pegmatitic granite dyke, east face of Minnie hill. Numbered circles indicate the approximate positions of analysis sites. 6(a) and (b) are interpreted as pegmatoidal zircons whereas (c) and (d) are interpreted as xenocrystic zircons. Corresponding ages to all spots are listed in Table 1.

Figure 7. Cathodoluminescence image of representative zircons from sample 191751: Migmatitic granite, 2km west of Red Rock. Note the euhedral rims and resorbed cores. Numbered circles indicate the approximate positions of analysis sites. Corresponding ages to all spots are listed in Table 2.

Figure 8 (a) Weighted average age plot for U-Pb age data from 191751 zircon rims; (b) Weighted average age plot for U-Pb age data from 191751 zircon cores. Highlighted are younger ages which may have lost Pb; (c) Concordia Plot for sample 155710. Ages are coloured relative to U concentration, illustrating Pb loss during a high grade magamatic event; (d) Condordia plot for sample 191763. Discordant ages are highlighted in red.

Figure 9: (a) See text (Sect. 4.1); (b) Dextral sigmaclast defined by fine grained feldspars and qtz. See text (Sect. 4.2); (c) Strong evidence for high temperatures, GBM recrystallisation. See text (Sect. 4.3)

Figure 10 (a) A garnet is embayed and surrounded by a corona of bladed and radiating cordierite. Lining these coronas are spinel and cordierite symplectites, which are entrained in a foliation. A later fracture, cross cuts foliation and has allowed hydrous alteration of garnet to biotite. (b) Garnets are embayed and surrounded by a corona of bladed and radiating cordierite. Lining these coronas are spinel and cordierite symplectites, which are entrained in a foliation roughly parallel to the photo base. Sillimanite crystals lying within the corona and are aligned with transport orientation.

Table Captions

Table 1. SHRIMP data set for 191751. D = Discordant, M = Metamorphic rims, I = Magamtic crystaillization, P = Radiogenic Pb loss (from c. 1160 magmatic population). Analyses marked D and P were not used in age calculations. 1st session (in black) 1σ error of mean: 0.75. 1σ external spot to spot error: 1.67. 2nd session (in red) 1σ error of mean: 0.45. 1σ external spot to spot error: 0.95.

Table 2. SHRIMP data set for 191763. D = Discordant, I = Magamtic crystaillization, Analyses marked D were not used in age calculations. 1σ error of mean: 0.37. 1σ external spot to spot error: 0.88.

Page left intentionally blank

Grp no.	*Spot no.*	*Grain .spot*	*^{238}U (ppm)*	*^{232}Th (ppm)*	*$^{232}Th/^{238}U$*	*f^{204} (%)*	*$^{238}U/^{206}Pb$*	*±1s*	*$^{207}Pb/^{206}Pb$*	*±1s*	*$^{238}U/^{206}Pb^*$*	*±1s*	*$^{207}Pb^*/^{206}Pb^*$*	*±1s*	*$^{238}U/^{206}Pb^*$ date (Ma)*	*±1s*	*$^{207}Pb^*/^{206}Pb^*$ date (Ma)*	*±1s*	*Disc (%)*
M	22	751-18.1	489	138	0.29	0.162	5.681	0.065	0.07520	0.00049	5.690	0.070	0.07385	0.00062	1044	14	1037	17	-0.6
~~D~~	~~18~~	~~751-16.1~~	~~64~~	~~62~~	~~0.99~~	~~0.564~~	~~4.997~~	~~0.096~~	~~0.07898~~	~~0.00139~~	~~5.025~~	~~0.100~~	~~0.07425~~	~~0.00239~~	~~1170~~	~~25~~	~~1048~~	~~65~~	~~-11.6~~
M	4	751-4.1	2553	463	0.19	0.016	5.490	0.095	0.07477	0.00021	5.491	0.103	0.07464	0.00022	1079	22	1059	6	-1.9
M	6	751-6.1	2069	506	0.25	0.006	5.538	0.096	0.07495	0.00024	5.538	0.104	0.07490	0.00024	1070	22	1066	6	-0.4
M	10	751-9.1	1008	350	0.36	0.204	5.656	0.099	0.07665	0.00036	5.668	0.108	0.07494	0.00050	1047	22	1067	13	1.8
M	1	751-1.1	2443	428	0.18	0.388	5.463	0.094	0.07821	0.00023	5.484	0.103	0.07495	0.00038	1080	22	1067	10	-1.2
M	9	751-8.1	2526	465	0.19	0.015	5.501	0.095	0.07510	0.00022	5.502	0.103	0.07497	0.00023	1077	22	1068	6	-0.8
M	2	751-2.1	1537	165	0.11	0.008	5.542	0.096	0.07511	0.00028	5.543	0.105	0.07504	0.00029	1069	22	1070	8	0.0
M	3	751-3.1	3302	128	0.04	0.002	5.417	0.093	0.07508	0.00019	5.417	0.102	0.07507	0.00019	1092	22	1070	5	-2.0
~~D~~	~~13~~	~~751-11.1~~	~~97~~	~~137~~	~~1.46~~	~~0.134~~	~~4.908~~	~~0.108~~	~~0.07719~~	~~0.00116~~	~~4.914~~	~~0.114~~	~~0.07606~~	~~0.00141~~	~~1194~~	~~30~~	~~1097~~	~~37~~	~~-8.9~~
P	14	751-12.1	1346	113	0.09	0.978	5.330	0.056	0.08517	0.00033	5.383	0.062	0.07694	0.00071	1098	14	1120	18	1.9
P	19	751-16.2	581	63	0.11	0.113	5.344	0.060	0.07792	0.00048	5.350	0.065	0.07697	0.00057	1105	15	1120	15	1.4
P	5	751-5.1	1018	112	0.11	0.421	5.310	0.093	0.08073	0.00035	5.333	0.102	0.07718	0.00060	1108	23	1126	16	1.6
I	16	751-14.1	186	199	1.10	0.124	4.763	0.065	0.07882	0.00080	4.769	0.069	0.07777	0.00096	1227	20	1141	25	-7.5
I	15	751-13.1	882	80	0.09	0.118	5.042	0.054	0.07898	0.00038	5.048	0.059	0.07799	0.00045	1165	15	1146	11	-1.6
I	7	751-6.2	506	105	0.21	0.209	5.092	0.092	0.07991	0.00048	5.102	0.099	0.07814	0.00063	1154	25	1151	16	-0.3
I	8	751-7.1	842	90	0.11	0.040	5.047	0.089	0.07858	0.00037	5.049	0.097	0.07824	0.00040	1165	24	1153	10	-1.0
I	20	751-17.1	628	71	0.12	0.162	5.200	0.058	0.07963	0.00046	5.208	0.063	0.07826	0.00058	1132	15	1154	15	1.9
I	21	751-17.2	132	141	1.11	0.000	4.900	0.074	0.07868	0.00094	4.900	0.077	0.07868	0.00094	1197	21	1164	24	-2.8
I	23	751-18.2	74	69	0.96	0.082	4.882	0.089	0.07952	0.00132	4.886	0.091	0.07882	0.00149	1200	25	1168	38	-2.8
I	12	751-10.1	110	124	1.16	0.281	5.105	0.108	0.08176	0.00112	5.119	0.115	0.07938	0.00155	1150	28	1182	39	2.7
I	17	751-15.1	123	142	1.20	0.000	4.737	0.073	0.07998	0.00100	4.737	0.076	0.07998	0.00100	1235	22	1197	25	-3.2
I	11	751-9.2	327	249	0.79	0.035	4.997	0.093	0.08077	0.00063	4.999	0.100	0.08048	0.00066	1175	26	1209	16	2.7

Table 1

Grp no.	Spot no.	Grain .spot	^{238}U (ppm)	^{232}Th (ppm)	$^{232}Th/^{238}U$	f^{204} (%)	$^{238}U/^{206}Pb$	±1s	$^{207}Pb/^{206}Pb$	±1s	$^{238}U/^{206}Pb^*$	±1s	$^{207}Pb^*/^{206}Pb^*$	±1s	$^{238}U/^{206}Pb^*$ date (Ma)	±1s	$^{207}Pb^*/^{206}Pb^*$ date (Ma)	±1s	Disc (%)
I	1	763-1.1	806	475	0.61	0.034	5.198	0.053	0.07732	0.00037	5.200	0.056	0.07704	0.00039	1134	13	1122	10	-1.0
I	2	763-2.1	873	614	0.73	0.037	5.125	0.052	0.07796	0.00036	5.127	0.055	0.07764	0.00038	1149	14	1138	10	-1.0
I	3	763-3.1	1096	956	0.90	0.044	5.116	0.051	0.07767	0.00032	5.118	0.054	0.07730	0.00034	1150	13	1129	9	-1.9
I	4	763-4.1	647	263	0.42	0.000	5.201	0.054	0.07785	0.00042	5.201	0.058	0.07785	0.00042	1134	14	1143	11	0.8
I	5	763-5.1	709	794	1.16	0.016	5.120	0.053	0.07715	0.00040	5.121	0.056	0.07702	0.00041	1150	14	1122	11	-2.5
I	6	763-6.1	261	94	0.37	0.000	5.198	0.062	0.07830	0.00066	5.198	0.065	0.07830	0.00066	1134	16	1154	17	1.8
D	7	763-7.1	546	1369	2.59	0.000	4.543	0.050	0.07711	0.00047	4.543	0.053	0.07711	0.00047	1282	17	1124	12	-14.1
I	8	763-8.1	821	459	0.58	-0.008	4.960	0.051	0.07829	0.00042	4.959	0.054	0.07836	0.00042	1184	14	1156	11	-2.4
I	9	763-9.1	874	1329	1.57	0.006	5.258	0.053	0.07748	0.00036	5.258	0.057	0.07743	0.00036	1122	13	1132	9	0.9
I	10	763-10.1	345	342	1.03	0.031	5.247	0.059	0.07751	0.00056	5.248	0.063	0.07725	0.00059	1124	15	1128	15	0.3
I	11	763-11.1	464	786	1.75	0.201	5.303	0.057	0.07868	0.00048	5.314	0.061	0.07699	0.00063	1112	14	1121	16	0.8
I	12	763-12.1	440	688	1.62	-0.012	5.337	0.058	0.07814	0.00050	5.336	0.061	0.07825	0.00051	1107	14	1153	13	4.0
I	13	763-13.1	528	1103	2.16	0.010	5.302	0.057	0.07699	0.00046	5.302	0.060	0.07691	0.00047	1114	14	1119	12	0.4
I	14	763-17.1	294	109	0.38	0.093	5.213	0.061	0.07819	0.00062	5.218	0.064	0.07740	0.00072	1130	15	1131	18	0.1
I	15	763-13.2	257	170	0.68	0.151	5.258	0.063	0.07971	0.00067	5.266	0.066	0.07843	0.00083	1121	15	1158	21	3.2
I	16	763-14.1	465	132	0.29	0.025	5.209	0.056	0.07748	0.00050	5.210	0.060	0.07727	0.00052	1132	14	1128	13	-0.3
D	17	763-15.1	259	89	0.36	0.063	5.057	0.061	0.07678	0.00065	5.060	0.064	0.07625	0.00072	1163	16	1102	19	-5.5
I	18	763-16.1	336	106	0.32	-0.046	5.127	0.058	0.07777	0.00056	5.125	0.061	0.07816	0.00060	1149	15	1151	15	0.2

Table 2

Page left intentionally blank

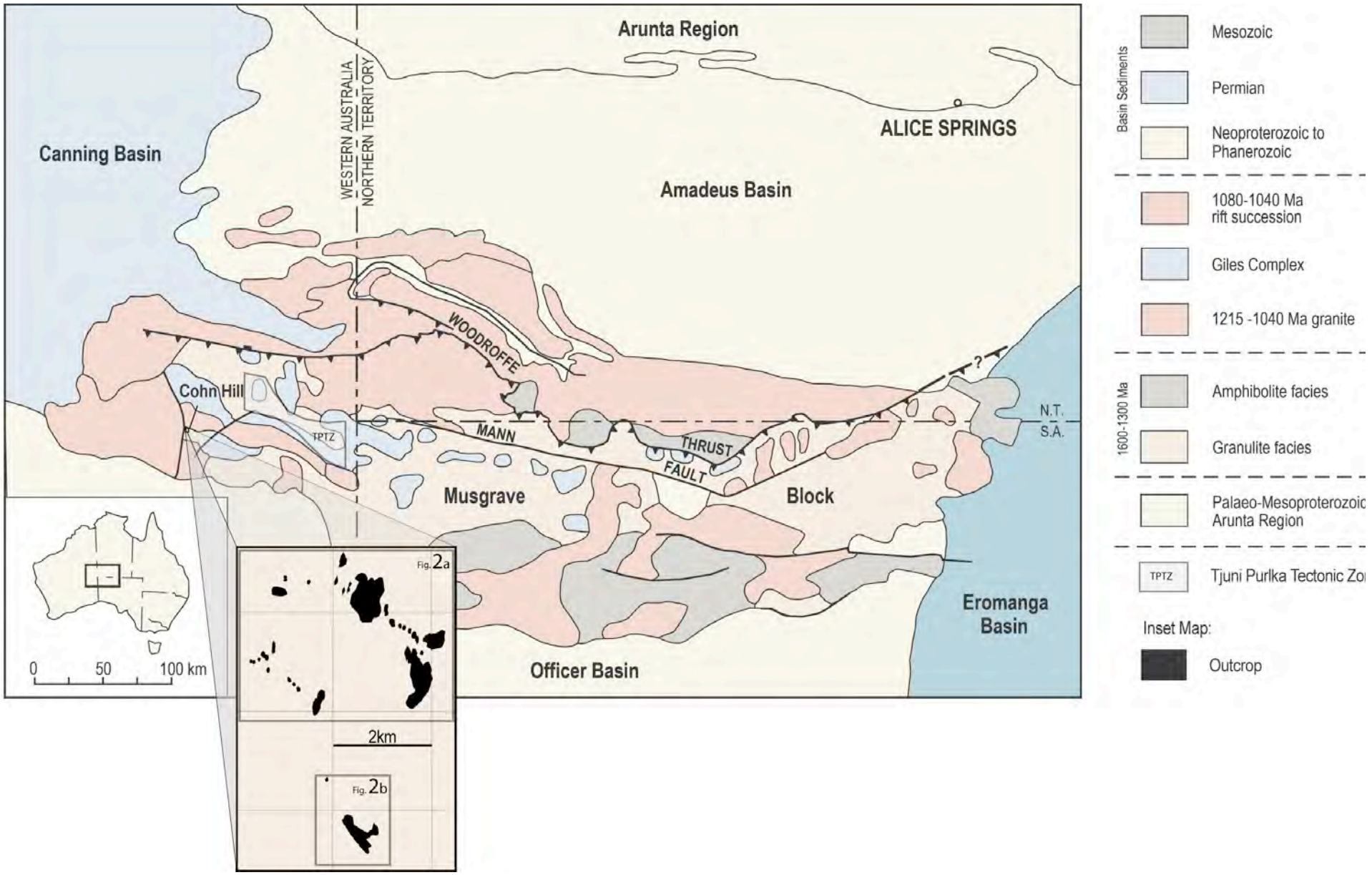
Arunta Region
ALICE SPRINGS
Canning Basin
WESTERN AUSTRALIA
NORTHERN TERRITORY
Amadeus Basin
WOODROFFE
Cohn Hill
TPTZ
MANN
THRUST
FAULT
N.T.
S.A.
Musgrave
Block
Eromanga
Basin
Officer Basin
0
50
100 km
Fig. 2a
2km
Fig. 2b
Basin Sediments
Mesozoic
Permian
Neoproterozoic to
Phanerozoic
1080-1040 Ma
rift succession
Giles Complex
1215 -1040 Ma granite
1600-1300 Ma
Amphibolite facies
Granulite facies
Palaeo-Mesoproterozoic
Arunta Region
TPTZ
Tjuni Purlka Tectonic Zo
Inset Map:
Outcrop

Figure 1

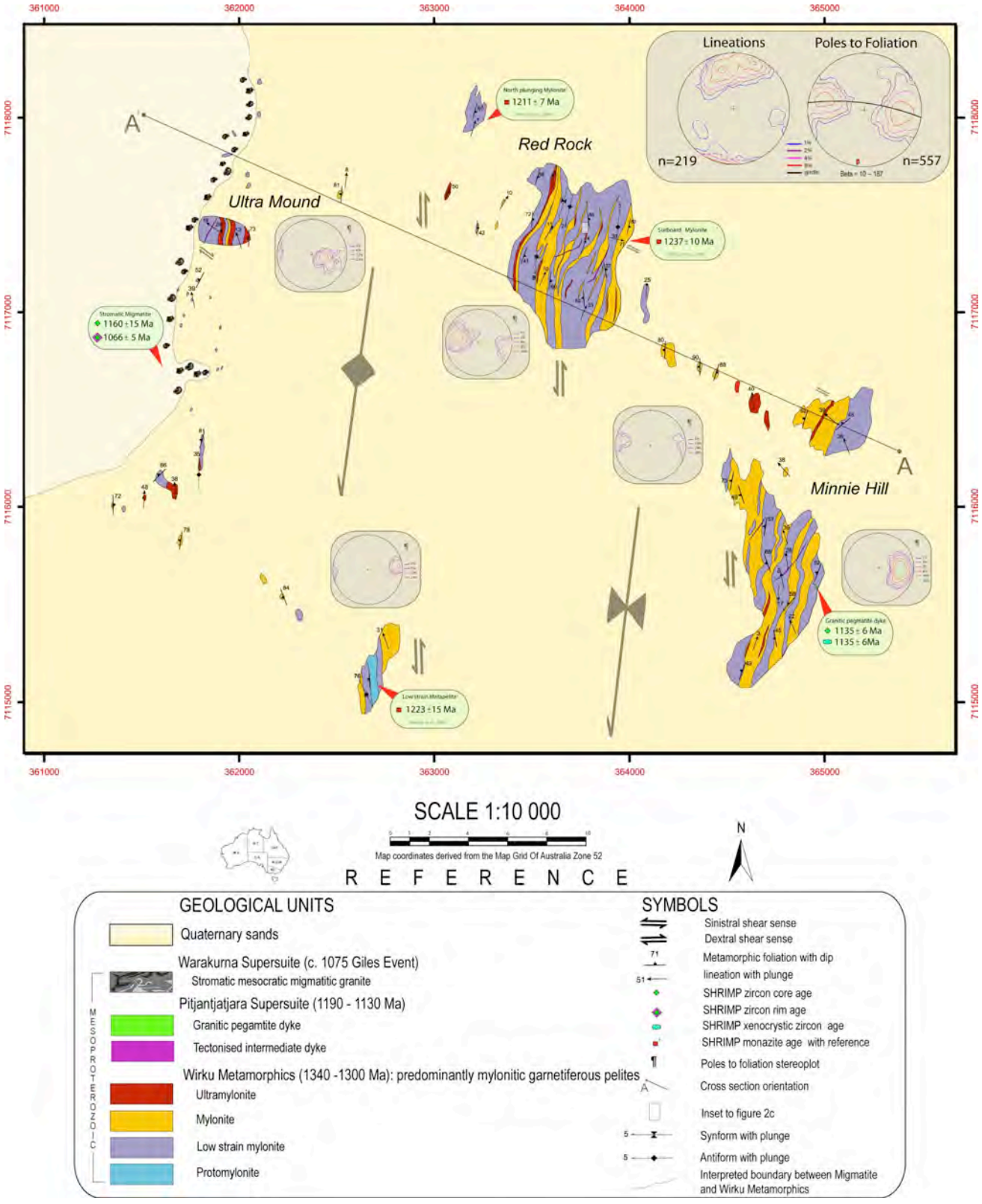
361000
362000
363000
364000
365000
7118000
7117000
7116000
7115000
Lineations
Poles to Foliation
n=219
n=557
Red Rock
Ultra Mound
Minnie Hill
A
A'
North plunging Mylonite
1211 ± 7 Ma
Subhorizontal Mylonite
1237 ± 10 Ma
Stromatic Migmatite
1160 ± 15 Ma
1066 ± 5 Ma
Low strain Metapelite
1223 ±15 Ma
Granitic pegmatite dyke
1135 ± 6 Ma
1135 ± 6Ma
SCALE 1:10 000
Map coordinates derived from the Map Grid Of Australia Zone 52
N
R E F E R E N C E
GEOLOGICAL UNITS
Quaternary sands
Warakurna Supersuite (c. 1075 Giles Event)
Stromatic mesocratic migmatitic granite
Pitjantjatjara Supersuite (1190 - 1130 Ma)
Granitic pegamtite dyke
Tectonised intermediate dyke
Wirku Metamorphics (1340 -1300 Ma): predominantly mylonitic garnetiferous pelites
Ultramylonite
Mylonite
Low strain mylonite
Protomylonite
MESOPROTEROZOIC
SYMBOLS
Sinistral shear sense
Dextral shear sense
Metamorphic foliation with dip
lineation with plunge
SHRIMP zircon core age
SHRIMP zircon rim age
SHRIMP xenocrystic zircon age
SHRIMP monazite age with reference
Poles to foliation stereoplot
Cross section orientation
Inset to figure 2c
Synform with plunge
Antiform with plunge
Interpreted boundary between Migmatite and Wirku Metamorphics

Figure 2 (a)

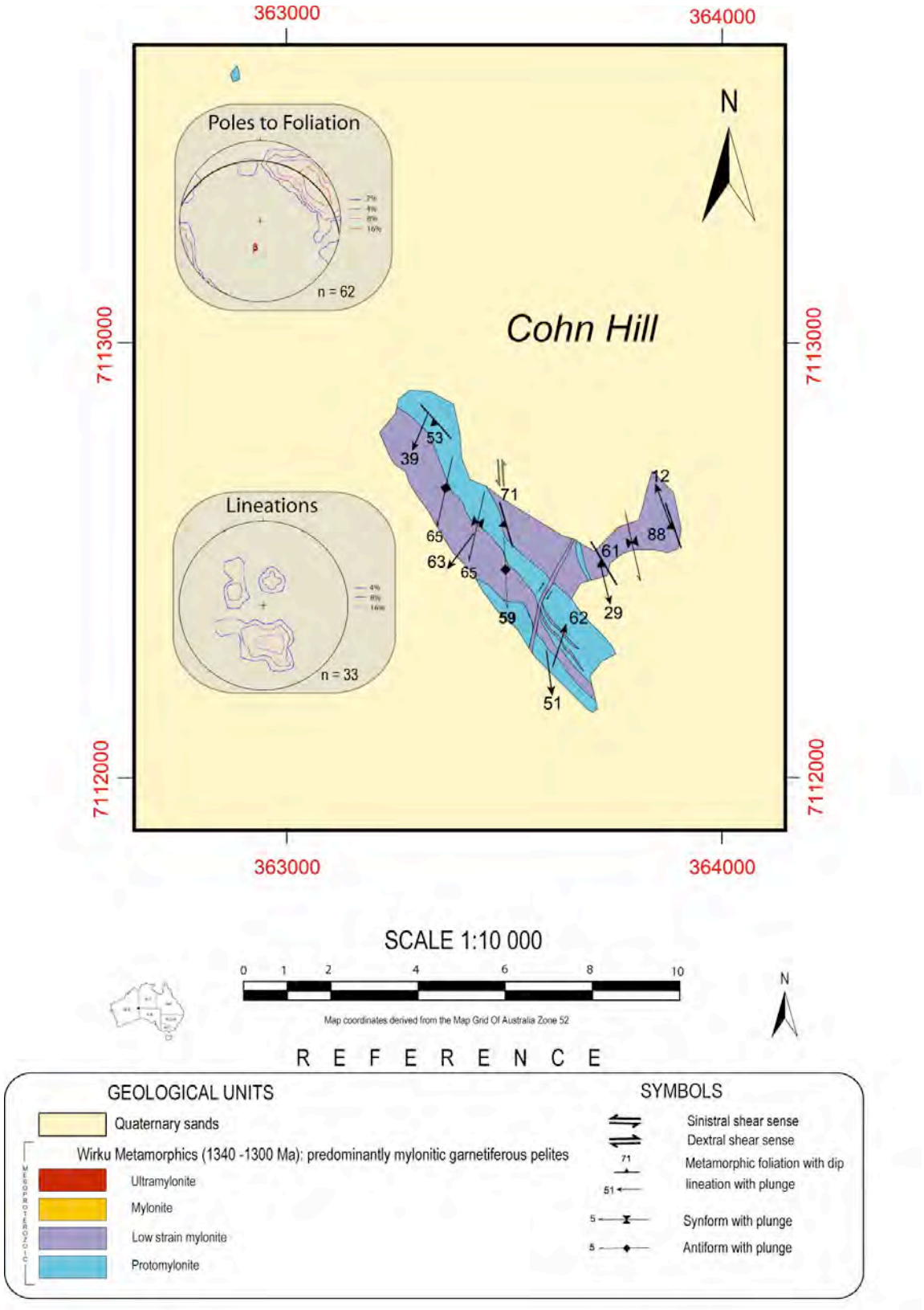
363000
364000
7113000
7112000
N
Poles to Foliation
n = 62
Cohn Hill
Lineations
n = 33
53
39
71
12
88
65
63
65
61
29
59
62
51
SCALE 1:10 000
0 1 2 4 6 8 10
Map coordinates derived from the Map Grid Of Australia Zone 52
R E F E R E N C E
GEOLOGICAL UNITS
Quaternary sands
Wirku Metamorphics (1340 -1300 Ma): predominantly mylonitic garnetiferous pelites
MESOPROTEROZOIC
Ultramylonite
Mylonite
Low strain mylonite
Protomylonite
SYMBOLS
Sinistral shear sense
Dextral shear sense
71
Metamorphic foliation with dip
51
lineation with plunge
5
Synform with plunge
5
Antiform with plunge

Figure 2 (b)

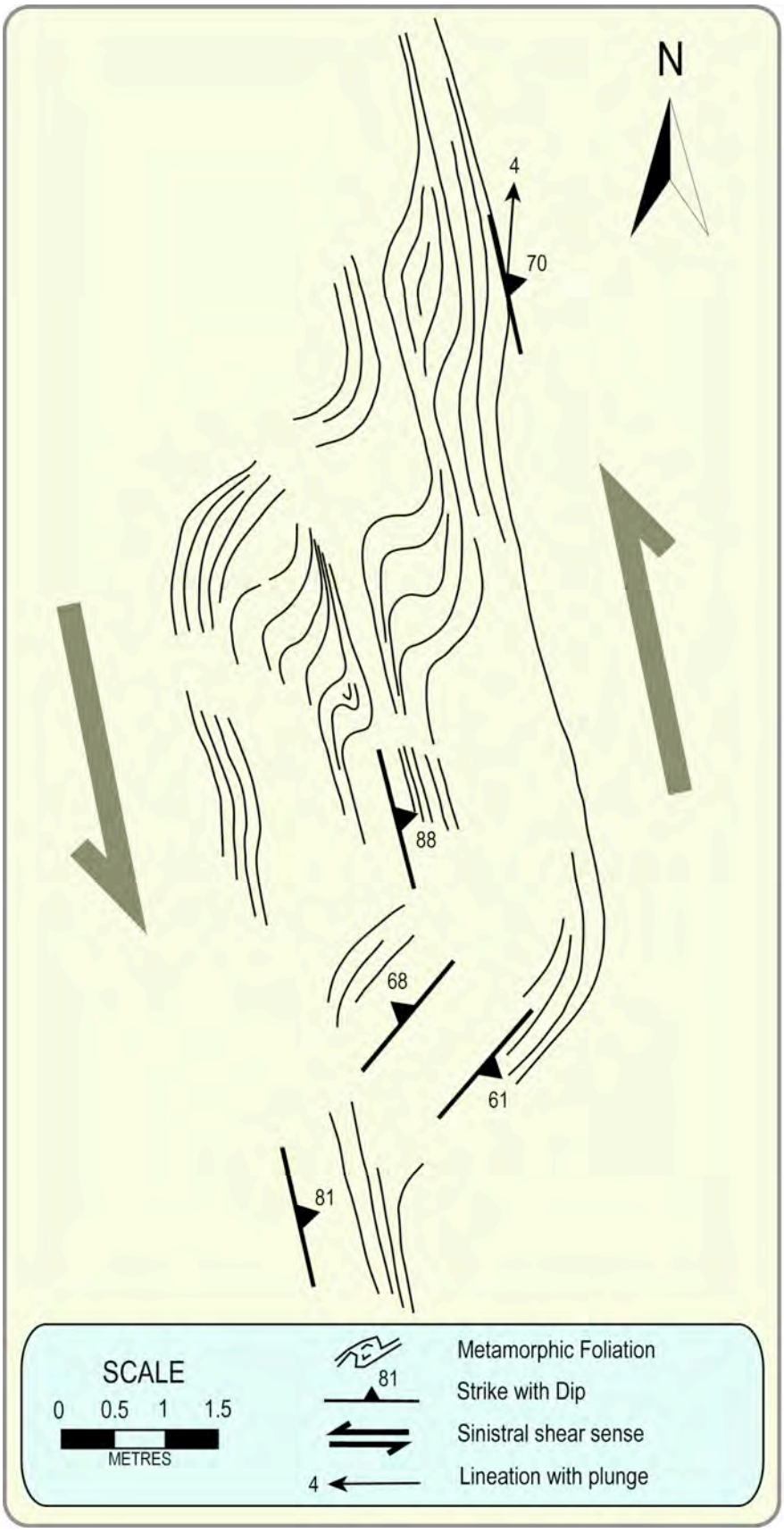
N
4
70
88
68
61
81
SCALE
0 0.5 1 1.5
METRES
Metamorphic Foliation
81
Strike with Dip
Sinistral shear sense
4
Lineation with plunge

Figure 2 (c)

Schematic Cross Section A to A'

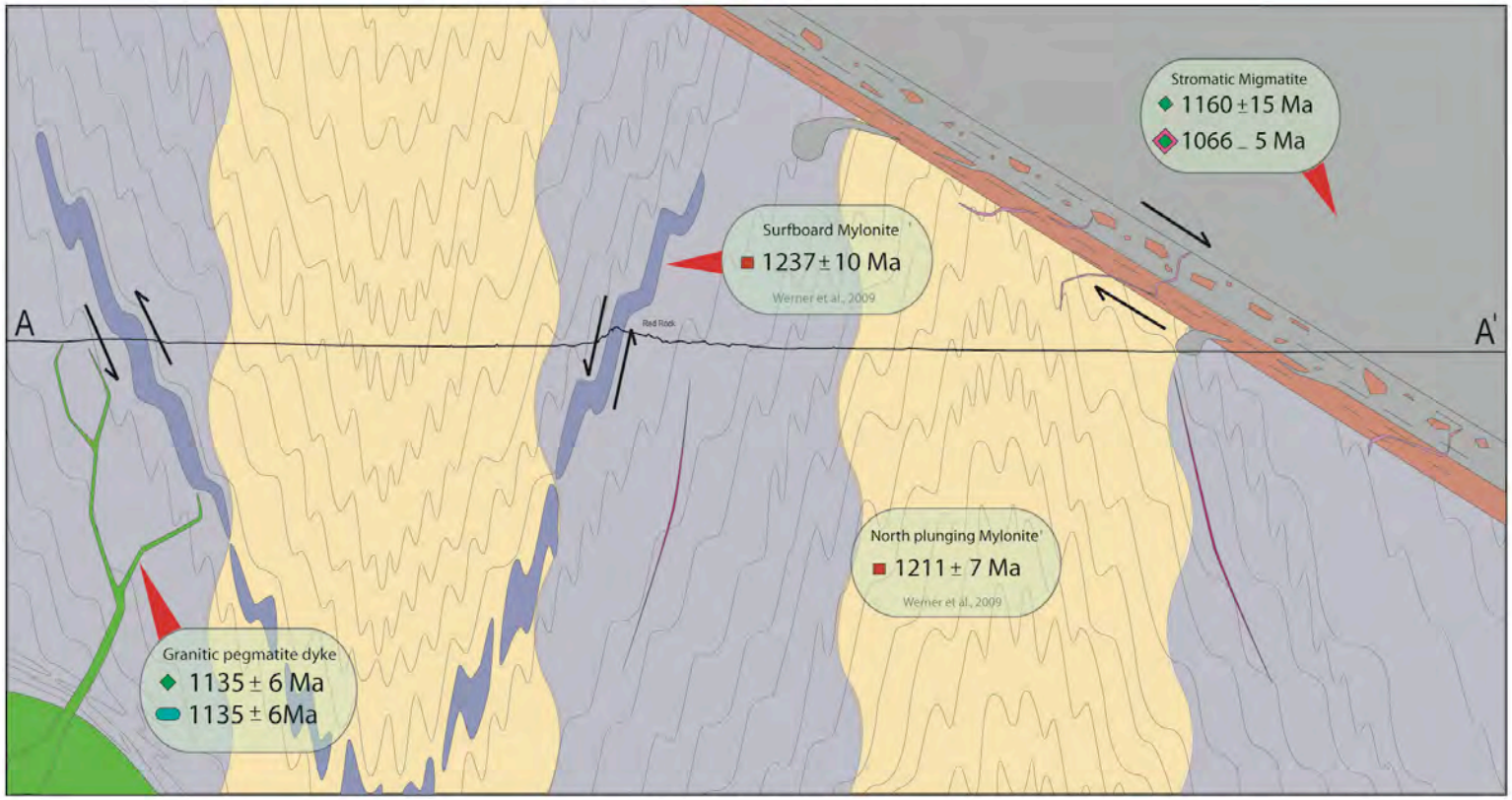

SCALE 1:10 000

Map coordinates derived from the Map Grid Of Australia Zone 52

East ⟵ ⟶ West

R E F E R E N C E

GEOLOGICAL UNITS

MESOPROTEROZOIC

Warakurna Supersuite (c. 1075 Giles Event)
- Stromatic mesocratic migmatitic granite
- Syntectonic granite vein

Pitjantjatjara Supersuite (1190 - 1130 Ma)
- Granitic pegamtite dyke
- tectonised intermediate dyke

Wirku Metamorphics (1340 -1300 Ma): predominantly mylonitic garnetiferous pelites
- Ultramylonite zone
- high strain zone
- low strain zone
- Preserved 'Surfboard' Mylonite

SYMBOLS
- Sinistral shear sense
- Dextral shear sense
- SHRIMP zircon core age
- SHRIMP zircon rim age
- SHRIMP xenocrystic zircon age
- SHRIMP monazite age with reference
- Cross section orientation
- Metamorphic foliation
- Present day topography

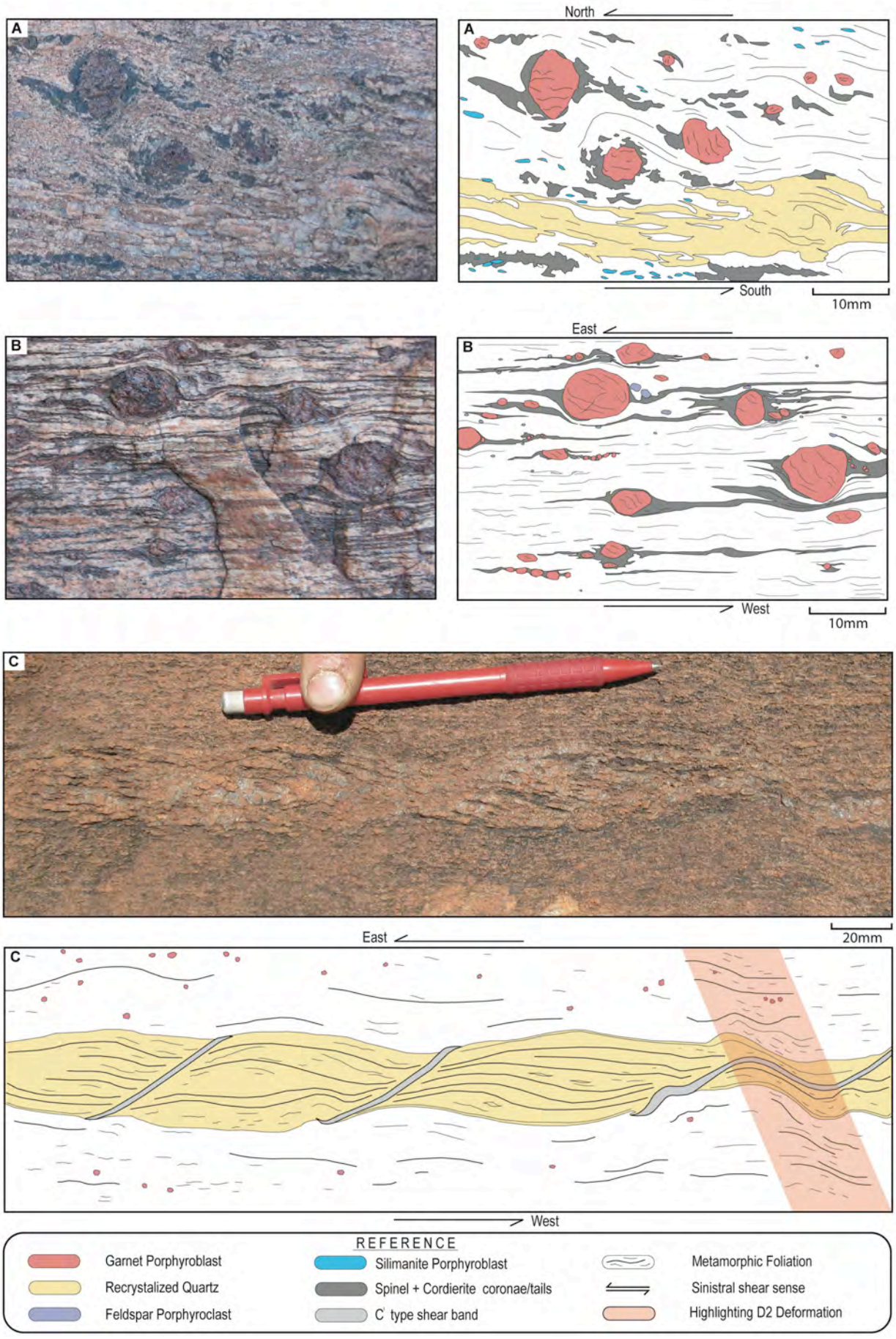
A
North
South
10mm
B
East
West
10mm
C
20mm
East
West
REFERENCE
Garnet Porphyroblast
Recrystalized Quartz
Feldspar Porphyroclast
Silimanite Porphyroblast
Spinel + Cordierite coronae/tails
C' type shear band
Metamorphic Foliation
Sinistral shear sense
Highlighting D2 Deformation

Figure 4 (a – c)

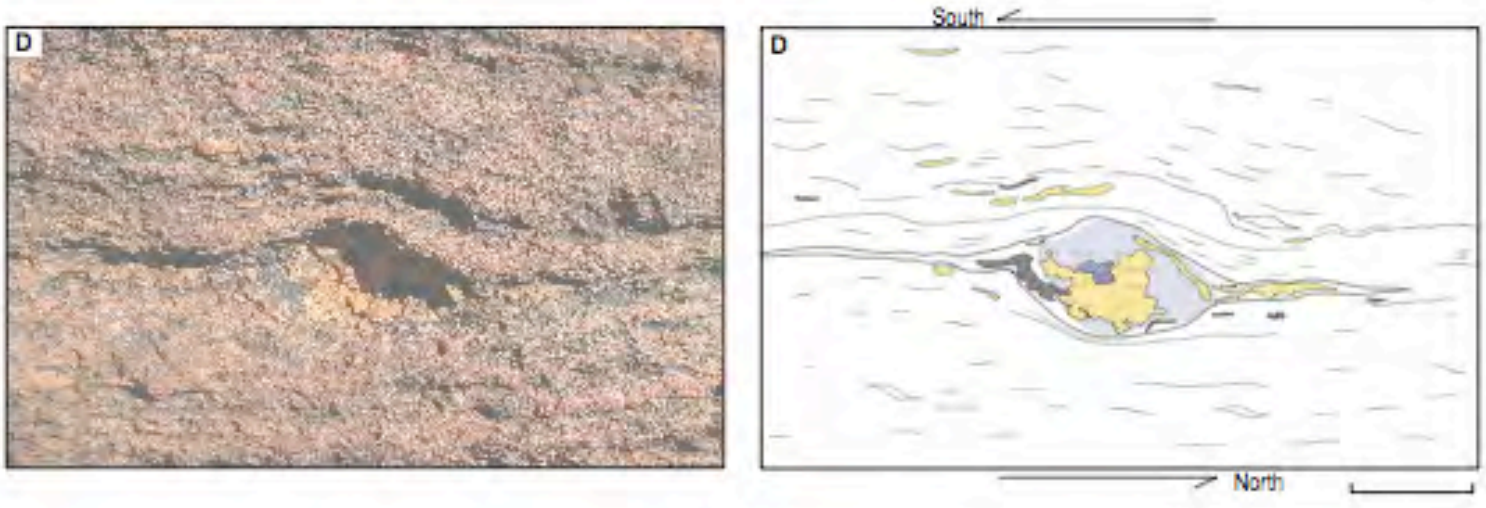

Figure 4 (d)

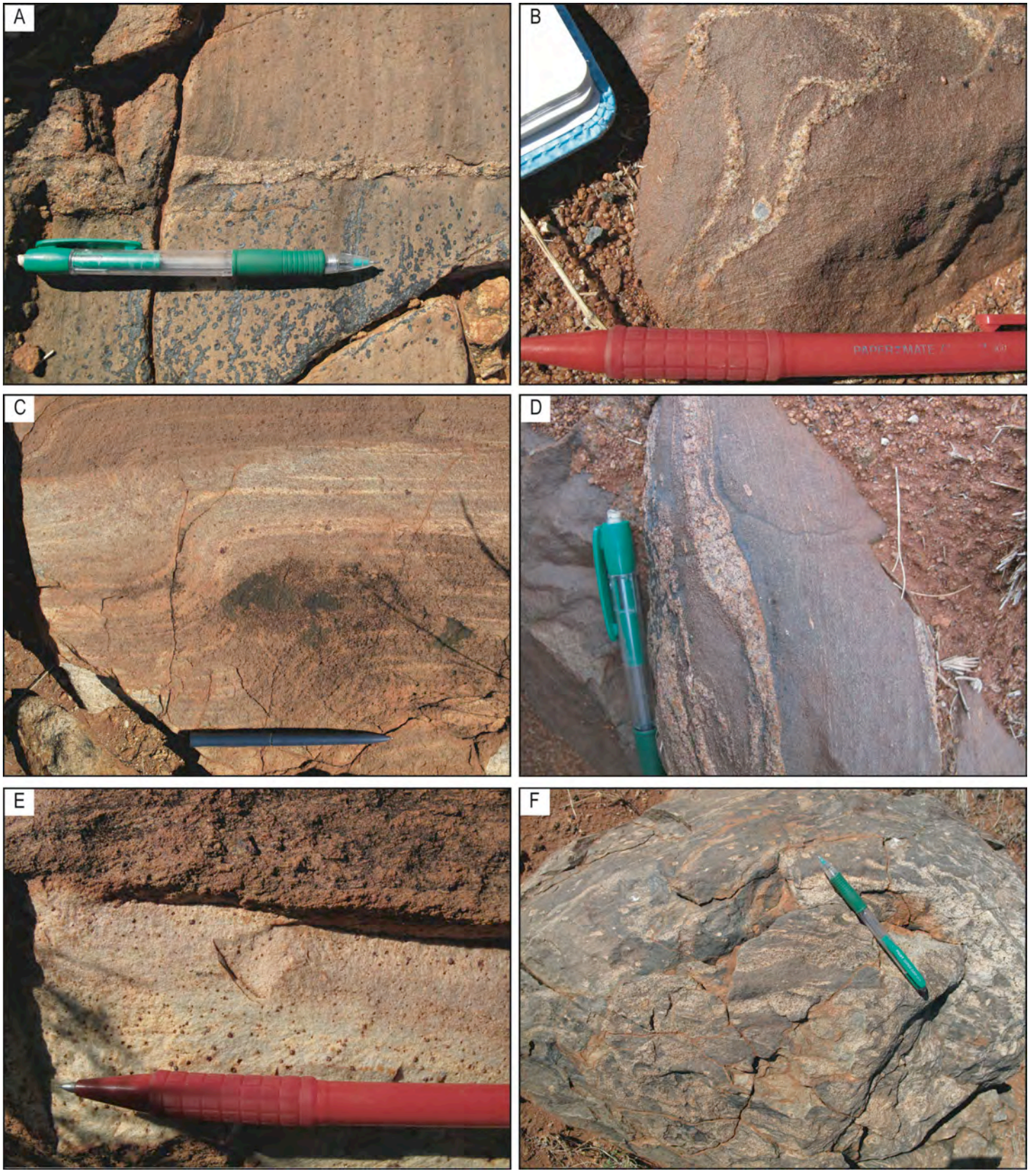

Figure 5 (a –f)

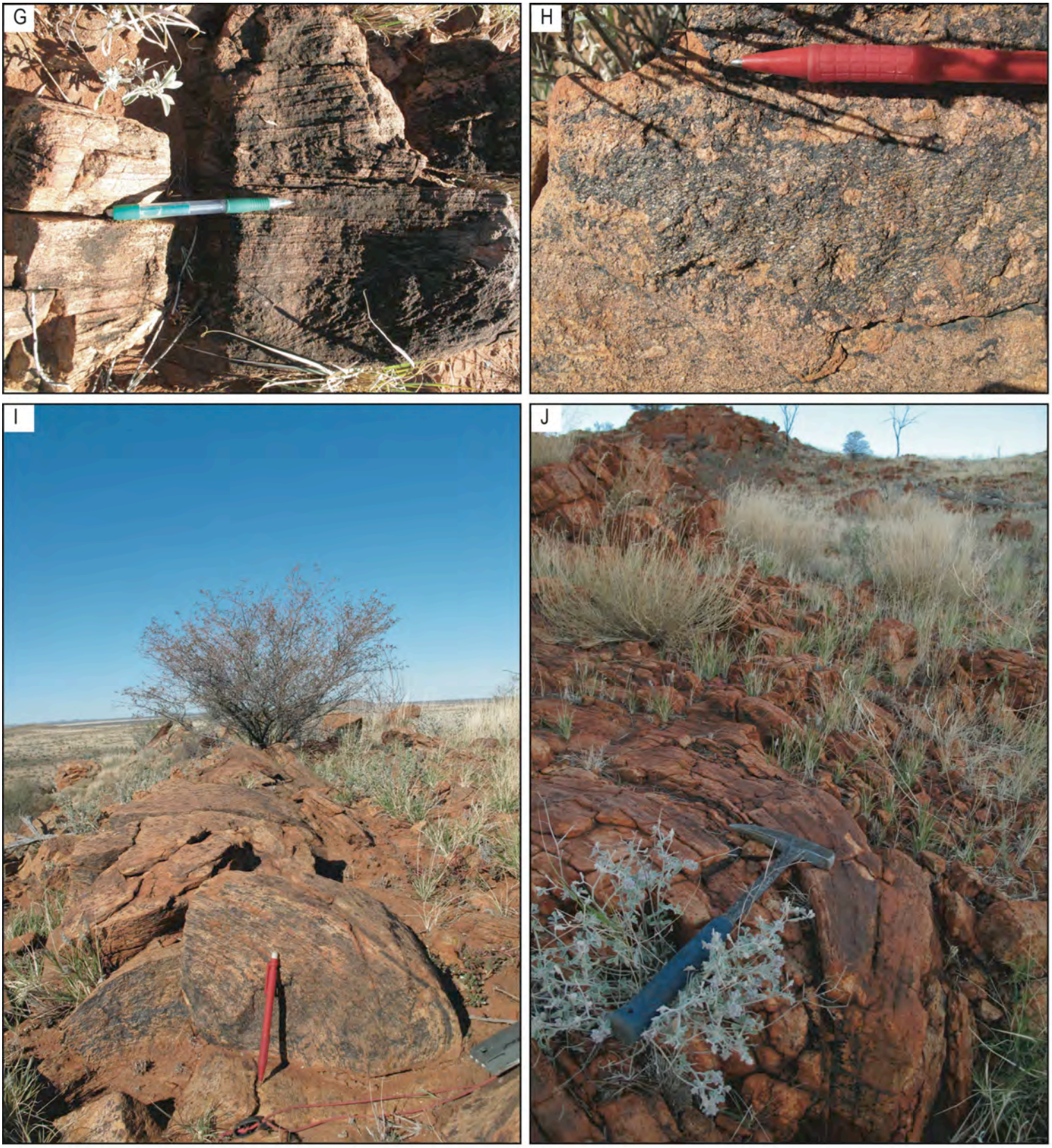

Figure 5 (g – j)

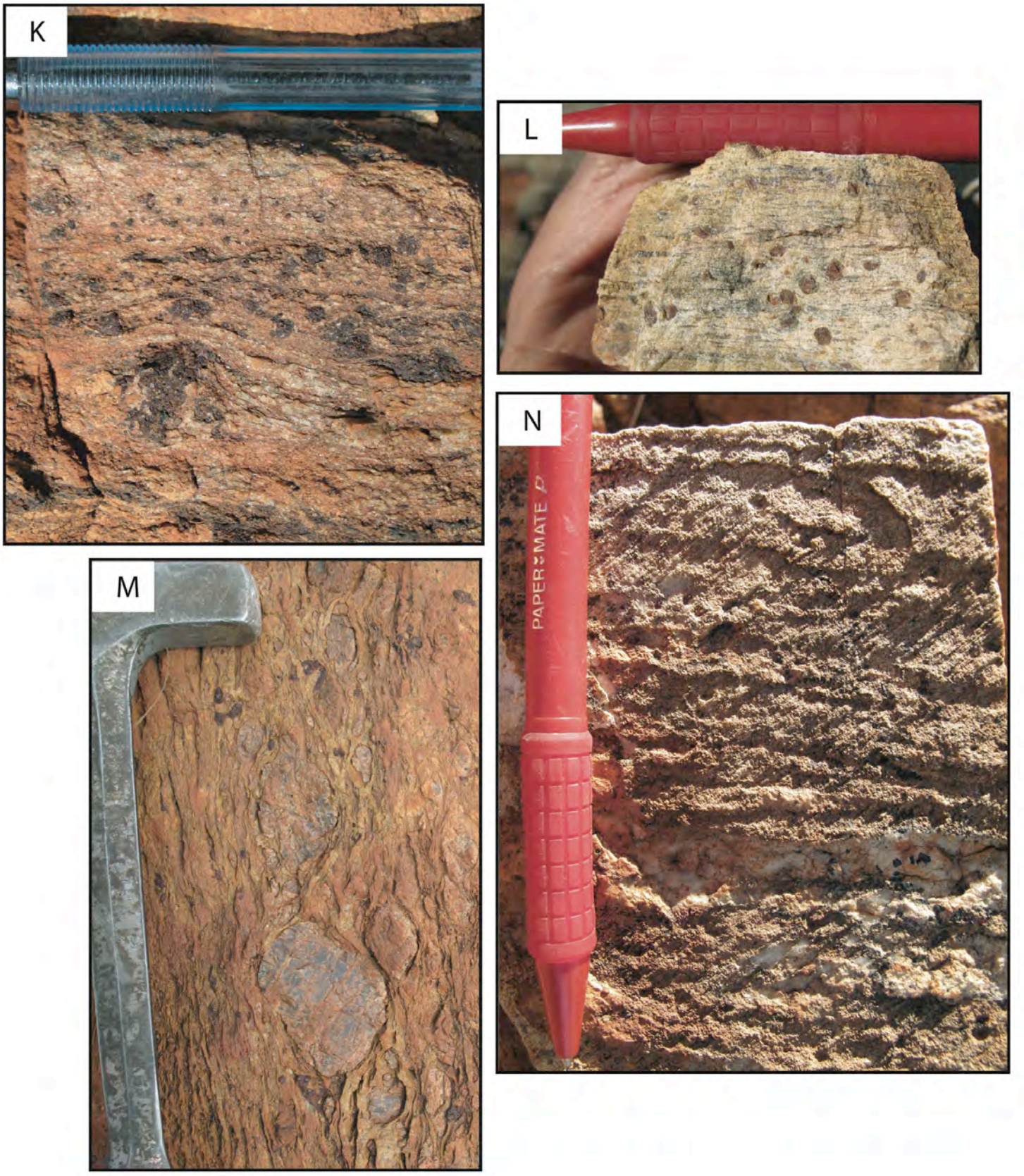

Figure 5 (k – n)

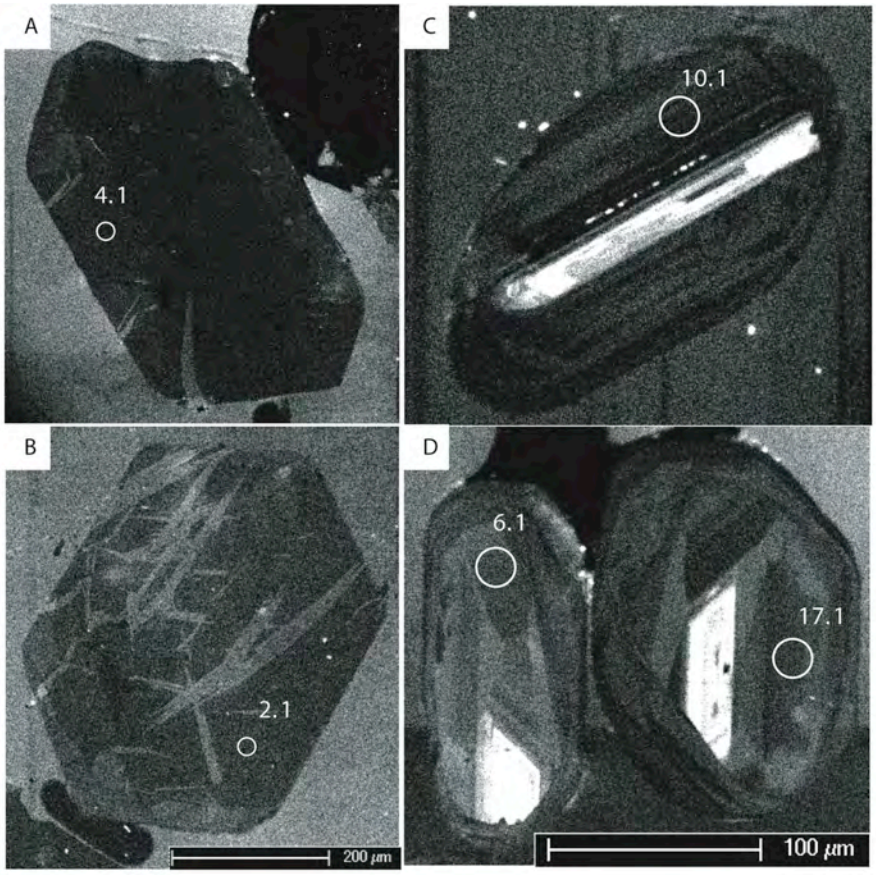

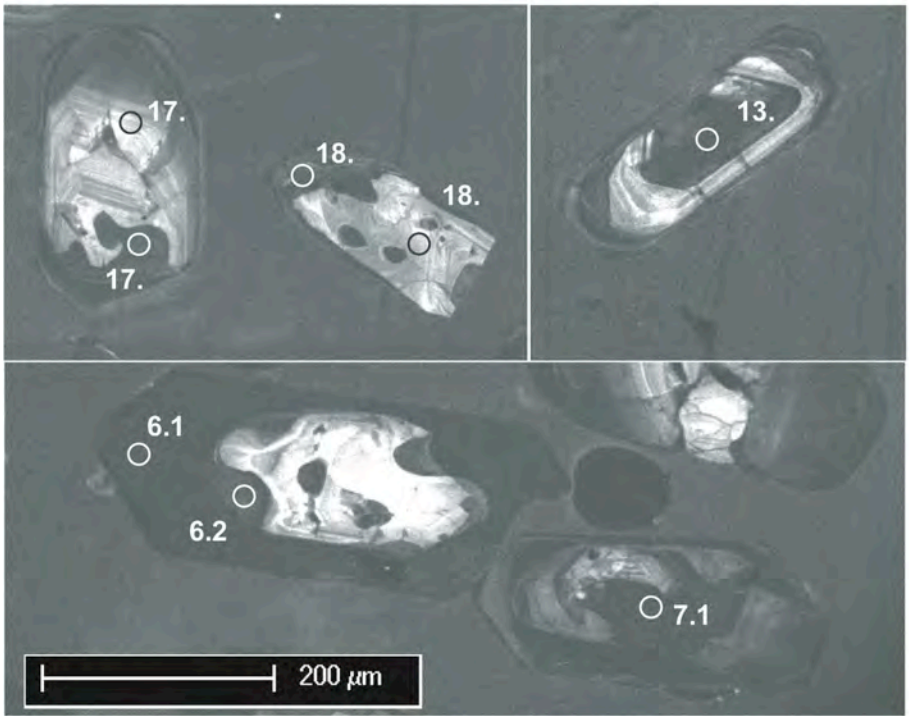

Figures 6 (a-d) and 7

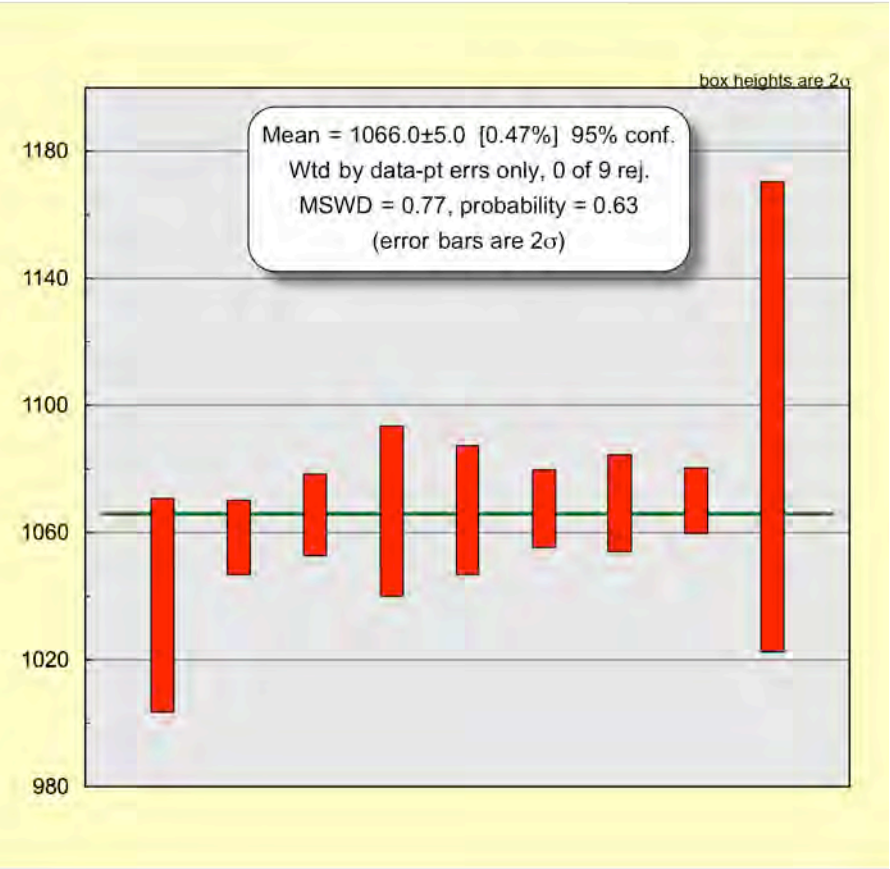
box heights are 2σ
Mean = 1066.0±5.0 [0.47%] 95% conf.
Wtd by data-pt errs only, 0 of 9 rej.
MSWD = 0.77, probability = 0.63
(error bars are 2σ)
1180
1140
1100
1060
1020
980

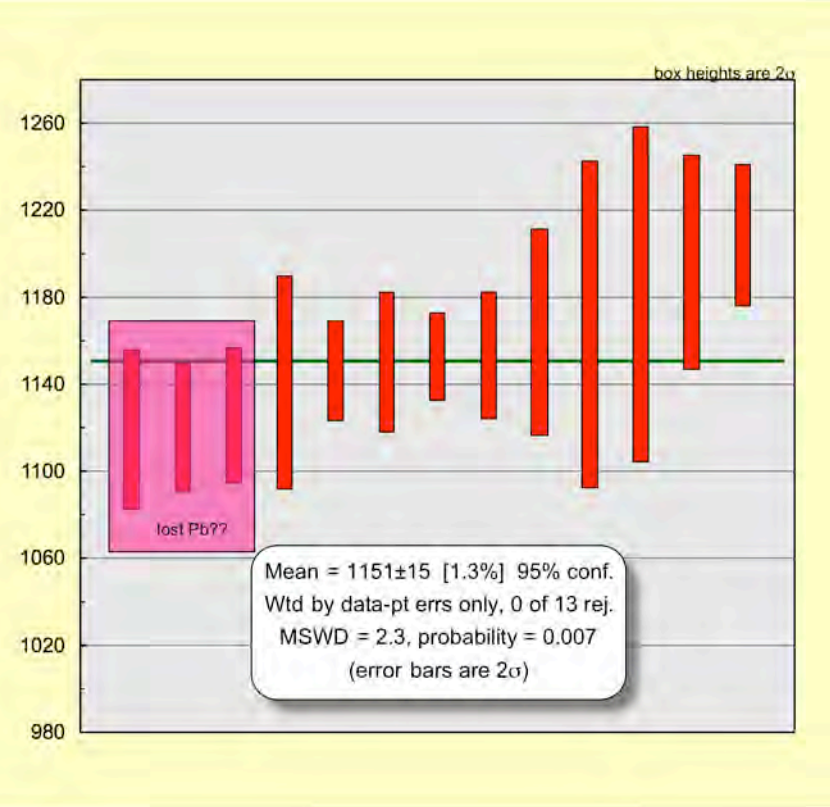
box heights are 2σ
1260
1220
1180
1140
1100
1060
1020
980
lost Pb??
Mean = 1151±15 [1.3%] 95% conf.
Wtd by data-pt errs only, 0 of 13 rej.
MSWD = 2.3, probability = 0.007
(error bars are 2σ)

Figure 8 (a – b)

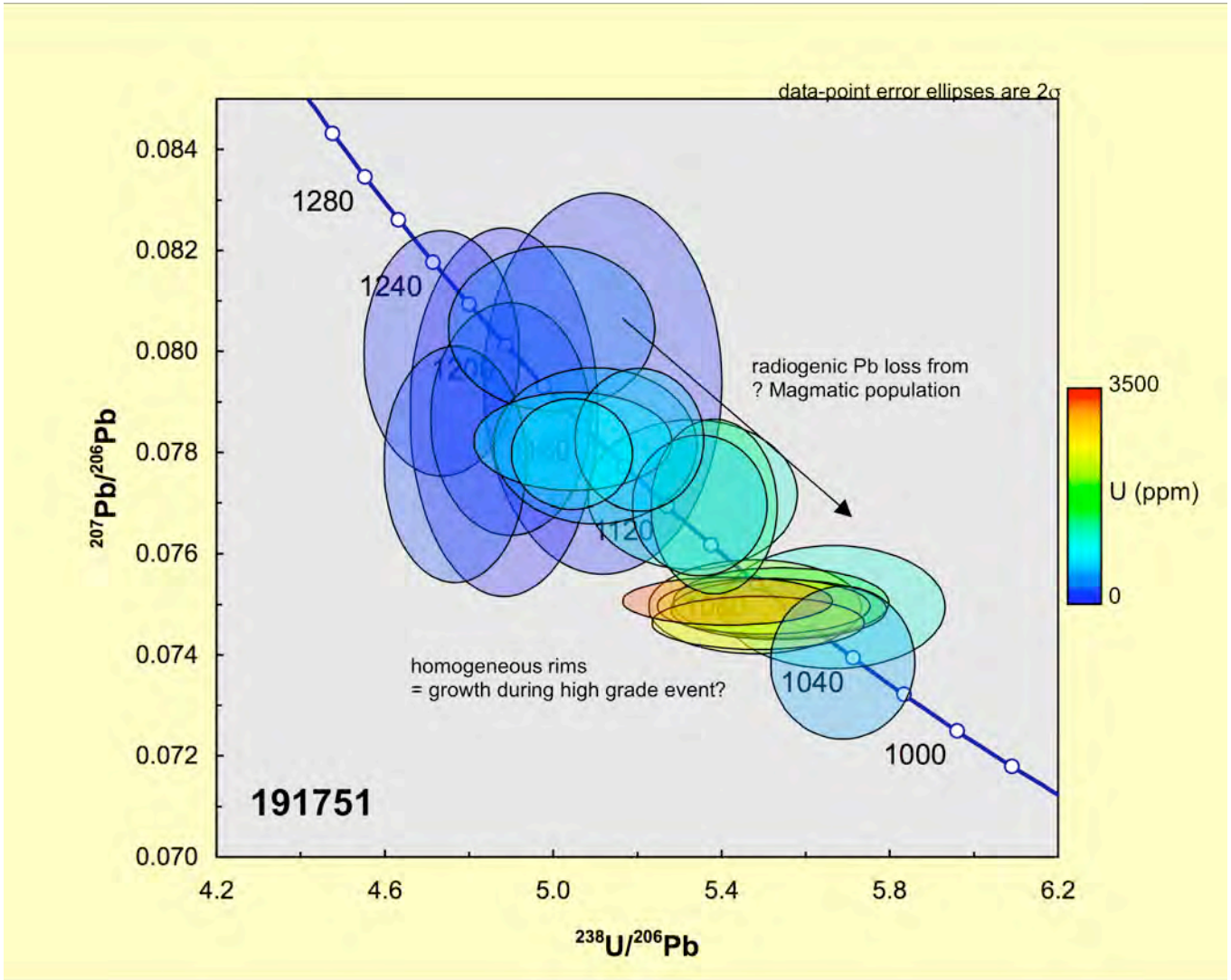
data-point error ellipses are 2σ
radiogenic Pb loss from
? Magmatic population
homogeneous rims
= growth during high grade event?
1280
1240
1200
1120
1040
1000
191751
3500
U (ppm)
0
0.084
0.082
0.080
0.078
0.076
0.074
0.072
0.070
4.2
4.6
5.0
5.4
5.8
6.2
207Pb/206Pb
238U/206Pb

Figure 8 (c)

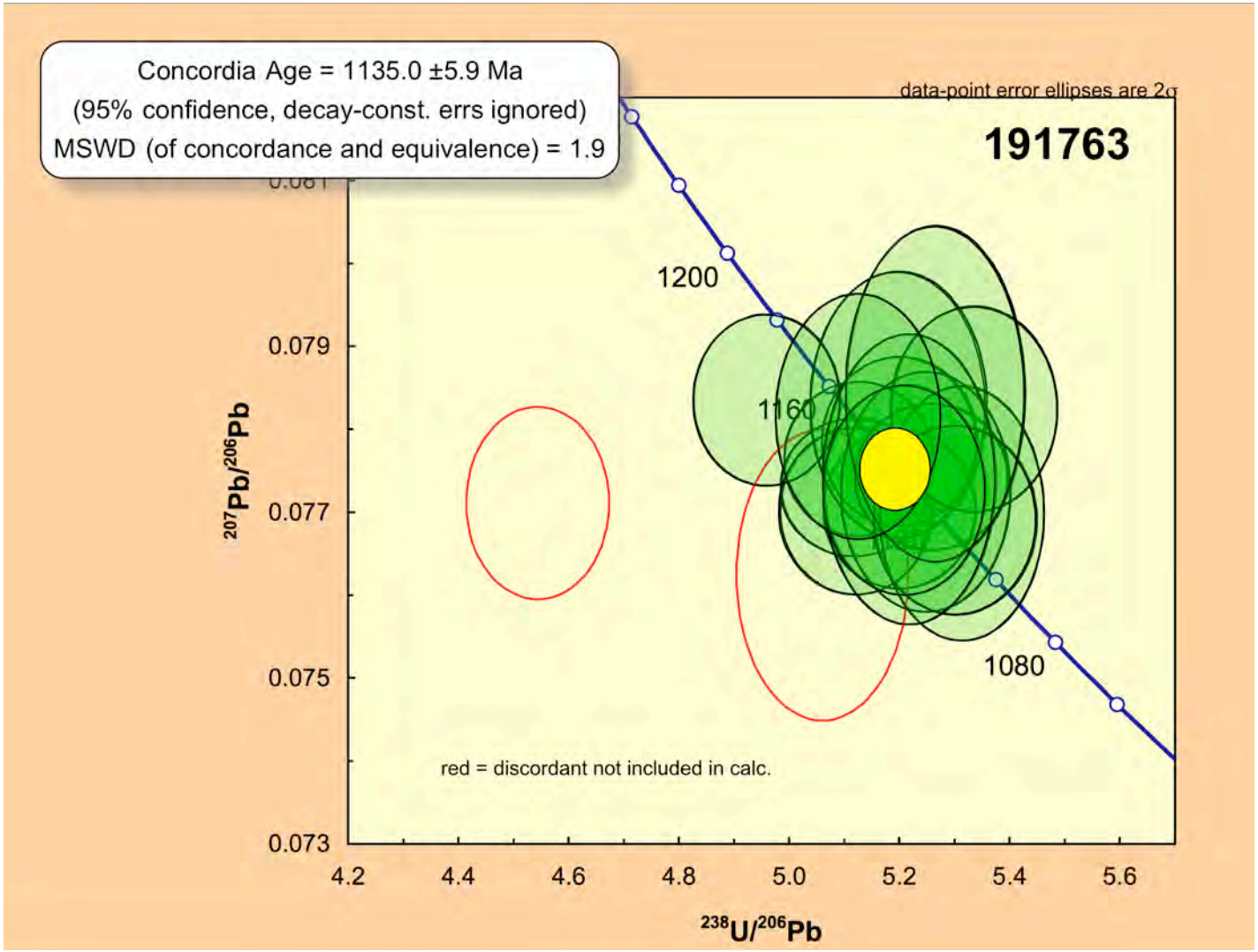
Concordia Age = 1135.0 ±5.9 Ma
(95% confidence, decay-const. errs ignored)
MSWD (of concordance and equivalence) = 1.9
data-point error ellipses are 2σ
191763
1200
1160
1080
red = discordant not included in calc.
0.079
0.077
0.075
0.073
4.2
4.4
4.6
4.8
5.0
5.2
5.4
5.6
207Pb/206Pb
238U/206Pb

Figure 8 (d)

Page intentionally left blank.

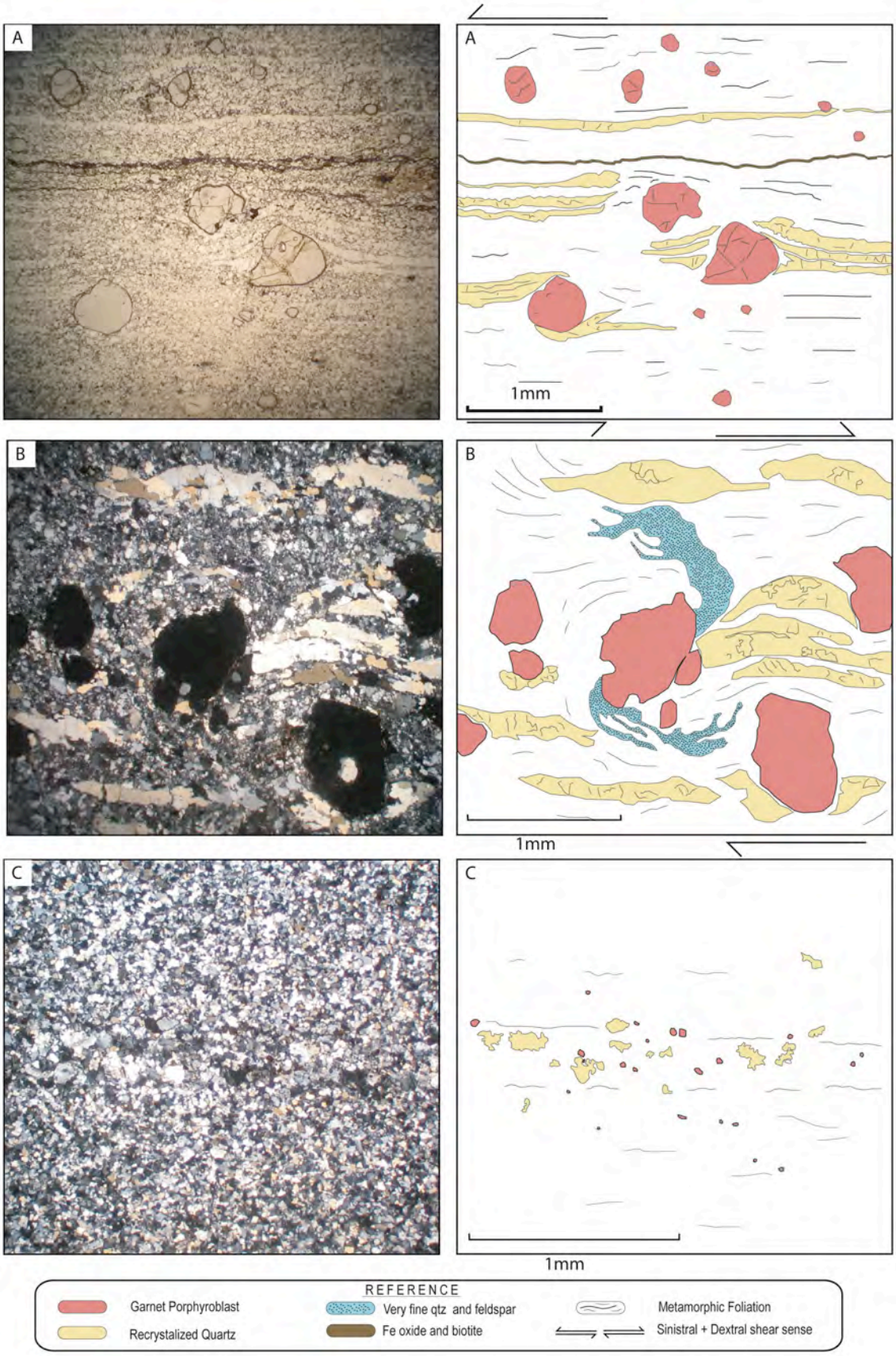
A
A
1mm
B
B
1mm
C
C
1mm
REFERENCE
Garnet Porphyroblast
Recrystalized Quartz
Very fine qtz and feldspar
Fe oxide and biotite
Metamorphic Foliation
Sinistral + Dextral shear sense

Figure 9 (a-c)

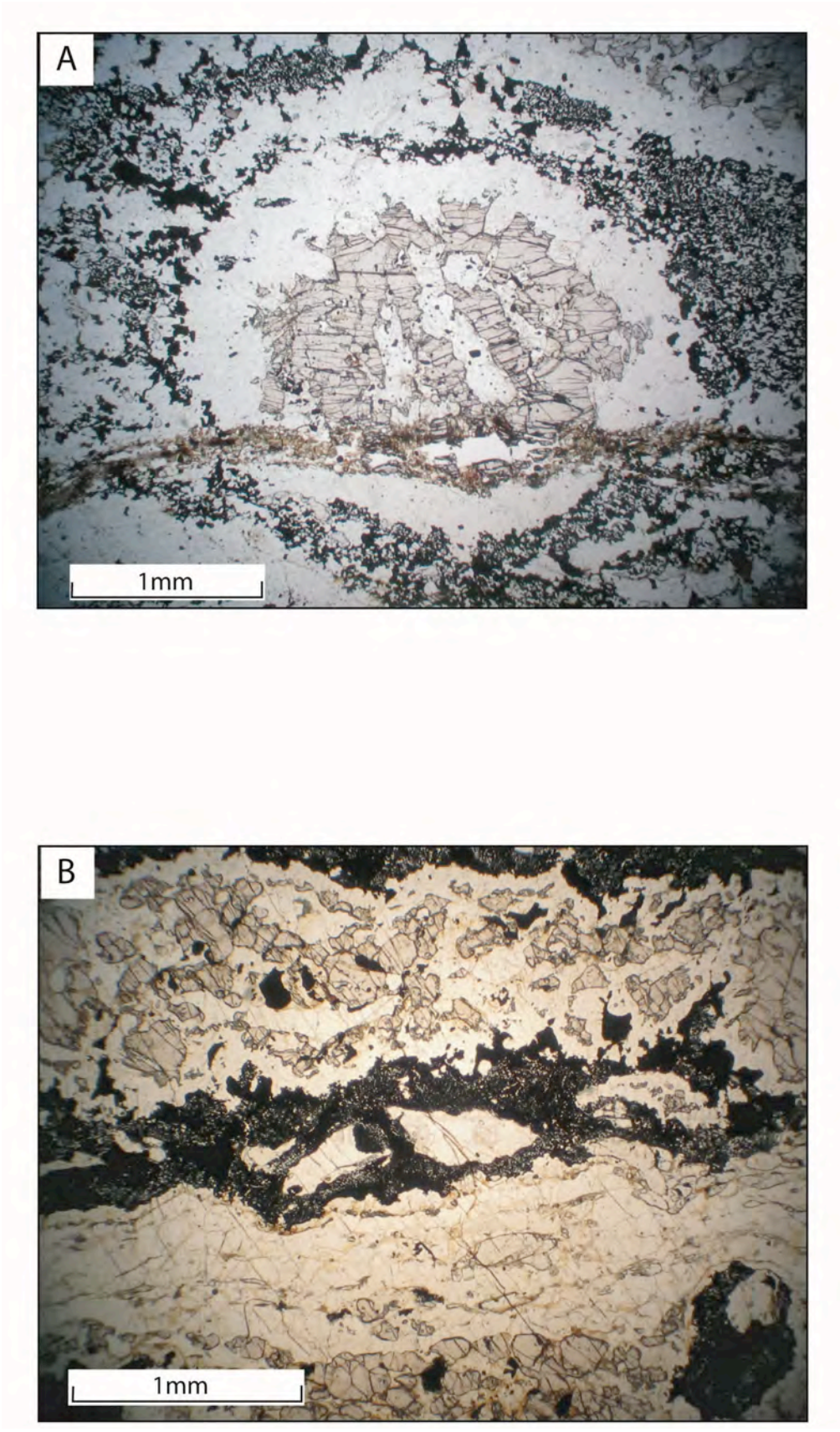

Figure 10 (a-b)

Appendix 1 – All foliations and lineations

All foliations

SITEID	STRUCTYPEID	DIP	P_AZIMUTH	location
AXSXXX307	FOIN	38	270	ULTMND
AXSXXX307	FOIN	59	300	ULTMND
AXSXXX307		49	312	ULTMND
AXSXXX309	FOIN	25	290	ULTMND
AXSXXX309	FOIN	24	285	ULTMND
		29	280	ULTMND
		25	290	ULTMND
AXSXXX310	FOIN	23	306	ULTMND
		32	278	ULTMND
AXSXXX311	FOIN	23	253	ULTMND
AXSXXX312	FOIN	41	271	ULTMND
AXSXXX313	FOIN	23	297	ULTMND
AXSXXX314	FOIN	18	315	ULTMND
		12	306	ULTMND
AXSXXX320	FOIN	62	302	ULTMND
AXSXXX323	FOIN	37	281	ULTMND
		29	329	ULTMND
AXSXXX325	FOIN	52	297	ULTMND
AXSXXX336	FOIN	81	286	ULTMND
		83	287	ULTMND
		85	105	ULTMND
AXSXXX337	FOIN	88	93	ULTMND
		87	90	ULTMND
AXSXXX338	FOIN	86	89	ULTMND
		82	93	ULTMND
AXSXXX339	FOIN	74	276	ULTMND
AXSXXX341	FOIN	29	286	ULTMND
		29	265	ULTMND
		30	286	ULTMND
AXSXXX342	FOIN	29	274	ULTMND
		24	296	ULTMND
		21	295	ULTMND
AXSXXX343	FOIN	24	296	ULTMND
		21	321	ULTMND
		43	298	ULTMND
AXSXXX344	FOIN	40	270	ULTMND
		45	297	ULTMND
		34	274	ULTMND
AXSXXX345	FOIN	73	271	ULTMND
		70	259	ULTMND
		50	284	ULTMND
		68	272	ULTMND
AXSXXX346	FOIN	53	315	ULTMND
AXSXXX347	FOIN	81	273	ULTMND
		86	286	ULTMND
AXSXXX348	FOIN	50	113	ULTMND
		66	116	ULTMND

Appendix 1 – All foliations and lineations

AXSXXX351	FOIN	60	105	Red Rock
		87	116	Red Rock
		90	114	Red Rock
AXSXXX352	FOIN	68	107	Red Rock
		70	109	Red Rock
AXSXXX353	FOIN	85	99	Red Rock
AXSXXX354	FOIN	43	95	Red Rock
		68	80	Red Rock
AXSXXX355	FOIN	68	80	Red Rock
AXSXXX356	FOIN	67	90	Red Rock
AXSXXX357	FOIN	42	95	Red Rock
AXSXXX358	FOIN	60	270	Red Rock
		27	139	Red Rock
		27	195	Red Rock
		50	244	Red Rock
AXSXXX360	FOIN	60	107	Red Rock
AXSXXX361	FOIN	51	93	Red Rock
		60	83	Red Rock
AXSXXX362	FOIN	35	90	Red Rock
AXSXXX363	FOIN	35	83	Red Rock
AXSXXX364	FOIN	60	105	Red Rock
AXSXXX365	FOIN	89	81	Red Rock
AXSXXX366	FOIN	88	110	Red Rock
AXSXXX367	FOIN	55	96	Red Rock
		64	91	Red Rock
		61	102	Red Rock
AXSXXX368	FOIN	51	120	Red Rock
		51	118	Red Rock
AXSXXX369	FOIN	60	114	Red Rock
AXSXXX370	FOIN	73	100	Red Rock
		71	105	Red Rock
		80	95	Red Rock
AXSXXX371	FOIN	83	102	Red Rock
		83	102	Red Rock
AXSXXX372	FOIN	64	108	Red Rock
		57	99	Red Rock
		73	98	Red Rock
		79	107	Red Rock
AXSXXX373	FOIN	68	296	Red Rock
		84	290	Red Rock
		69	295	Red Rock
AXSXXX374	FOIN	86	294	Red Rock
		84	274	Red Rock
		64	296	Red Rock
AXSXXX375	FOIN	85	271	Red Rock
		70	270	Red Rock
AXSXXX376	FOIN	83	90	Red Rock
AXSXXX377	FOIN	30	83	Red Rock
		32	63	Red Rock
		33	106	Red Rock

Appendix 1 – All foliations and lineations

		27	102	Red Rock
AXSXXX378	FOIN	79	276	Red Rock
		80	278	Red Rock
		70	281	Red Rock
AXSXXX381	FOIN	65	208	Red Rock
AXSXXX381	FOIN			Red Rock
AXSXXX382	FOIN	67	122	Red Rock
AXSXXX383	FOIN	85	270	Red Rock
		49	90	Red Rock
AXSXXX384	FOIN	47	90	Red Rock
		56	85	Red Rock
		61	81	Red Rock
AXSXXX385	FOIN	61	81	Red Rock
AXSXXX386	FOIN	32	79	Red Rock
AXSXXX387	FOIN	75	130	Red Rock
AXSXXX388	FOIN	74	106	Red Rock
AXSXXX389	FOIN	41	114	Red Rock
AXSXXX390	FOIN	76	96	Red Rock
		45	81	Red Rock
AXSXXX391	FOIN	59	84	Red Rock
AXSXXX392	FOIN	79	96	Red Rock
AXSXXX393	FOIN	87	106	Red Rock
AXSXXX395	FOIN	62	91	Red Rock
		59	251	Red Rock
		84	82	Red Rock
AXSXXX396	FOIN	64	131	Red Rock
AXSXXX397	FOIN	52	266	Red Rock
AXSXXX398	FOIN	58	112	Red Rock
AXSXXX399	FOIN	51	110	Red Rock
AXSXXX400	FOIN	69	110	Red Rock
AXSXXX401	FOIN	22	106	Red Rock
AXSXXX402	FOIN	58	90	Red Rock
		60	68	Red Rock
		52	92	Red Rock
AXSXXX403	FOIN	68	95	Red Rock
		62	94	Red Rock
AXSXXX404	FOIN	53	113	Red Rock
AXSXXX405	FOIN	43	87	Red Rock
AXSXXX406	FOIN	60	96	Red Rock
		51	98	Red Rock
		62	99	Red Rock
AXSXXX407	FOIN	45	106	Red Rock
		45	103	Red Rock
		58	112	Red Rock
		58	110	Red Rock
AXSXXX408	FOIN	69	106	Red Rock
		70	107	Red Rock
AXSXXX410	FOIN	79	280	Red Rock
AXSXXX411	FOIN	70	102	Red Rock
		75	104	Red Rock
		40	96	Red Rock

Appendix 1 – All foliations and lineations

		41	114	Red Rock
AXSXXX412	FOIN	41	110	Red Rock
		30	110	Red Rock
AXSXXX413	FOIN	79	102	Red Rock
		71	108	Red Rock
		68	102	Red Rock
AXSXXX414	FOIN	72	100	Red Rock
AXSXXX415	FOIN	42	90	Red Rock
AXSXXX416	FOIN	58	128	Red Rock
AXSXXX418	FOIN	68	116	Red Rock
AXSXXX420	FOIN	72	104	Red Rock
				Red Rock
AXSXXX556	FOIN	45	107	Red Rock
AXSXXX557	FOIN	72	94	Red Rock
		71	97	Red Rock
AXSXXX558	FOIN	53	109	Red Rock
AXSXXX559	FOIN	49	111	Red Rock
		52	113	Red Rock
AXSXXX560	FOIN	33	102	Red Rock
		30	97	Red Rock
		37	106	Red Rock
		23	121	Red Rock
		23	149	Red Rock
		21	155	Red Rock
		17	157	Red Rock
		53	118	Red Rock
		82	109	Red Rock
		59	107	Red Rock
		33	102	Red Rock
				Red Rock
AXSXXX561	FOIN	46	98	Red Rock
		47	110	Red Rock
AXSXXX562	FOIN	51	116	Red Rock
		50	117	Red Rock
AXSXXX563	FOIN	53	105	Red Rock
AXSXXX564	FOIN	76	285	Red Rock
		48	113	Red Rock
		46	121	Red Rock
		69	118	Red Rock
		69	164	Red Rock
		78	157	Red Rock
		79	307	Red Rock
		76	285	Red Rock
		83	270	Red Rock
AXSXXX565	FOIN	69	91	Red Rock
		78	95	Red Rock
AXSXXX566	FOIN	59	109	Red Rock
		68	103	Red Rock
		73	102	Red Rock
		72	107	Red Rock
		69	103	Red Rock

Appendix 1 – All foliations and lineations

AXSXXX567	FOIN	67	107	Red Rock
AXSXXX568	FOIN	64	90	Red Rock
		70	102	Red Rock
		61	87	Red Rock
AXSXXX569	FOIN	80	287	Red Rock
AXSXXX570	FOIN	77	286	Red Rock
AXSXXX571	FOIN	66	100	Red Rock
		62	106	Red Rock
AXSXXX572	FOIN	61	97	Red Rock
AXSXXX573	FOIN	67	100	Red Rock
AXSXXX574	FOIN	62	100	Red Rock
AXSXXX575	FOIN	68	119	Red Rock
AXSXXX576	FOIN	85	117	Red Rock
AXSXXX577	FOIN	71	110	Red Rock
		74	111	Red Rock
AXSXXX578	FOIN	69	111	Red Rock
AXSXXX579	FOIN	50	107	Red Rock
AXSXXX580	FOIN	59	111	Red Rock
AXSXXX581	FOIN	49	99	Red Rock
		63	106	Red Rock
AXSXXX582	FOIN	79	98	Red Rock
AXSXXX583	FOIN	82	273	Red Rock
AXSXXX584	FOIN	70	98	Red Rock
		81	100	Red Rock
		69	94	Red Rock
		69	104	Red Rock
AXSXXX585	FOIN	47	271	Red Rock
		68	270	Red Rock
		74	289	Red Rock
		79	106	Red Rock
AXSXXX586	FOIN	84	276	Red Rock
		66	276	Red Rock
		55	279	Red Rock
		49	69	Red Rock
AXSXXX588	FOIN	63	109	Red Rock
		60	276	Red Rock
		60	287	Red Rock
AXSXXX589	FOIN	61	121	Red Rock
		64	144	Red Rock
		71	138	Red Rock
AXSXXX590	FOIN	68	126	Red Rock
		44	113	Red Rock
		48	97	Red Rock
AXSXXX591	FOIN	43	113	Red Rock
		43	109	Red Rock
AXSXXX592	FOIN	43	107	Red Rock
AXSXXX593	FOIN	37	115	Red Rock
AXSXXX594	FOIN	41	126	Red Rock
AXSXXX595	FOIN	42	108	Red Rock
		46	116	Red Rock
AXSXXX596	FOIN	55	113	Red Rock

Appendix 1 – All foliations and lineations

		51	119	Red Rock
AXSXXX597	FOIN	52	107	Red Rock
AXSXXX598	FOIN	43	107	Red Rock
AXSXXX599	FOIN	81	109	Red Rock
AXSXXX600	FOIN	59	123	Red Rock
AXSXXX601	FOIN	82	294	Red Rock
		67	287	Red Rock
AXSXXX602	FOIN	33	104	Red Rock
AXSXXX603	FOIN	43	91	Red Rock

AXSXXX421	FOIN	81	90	noMNSLD
		83	97	noMNSLD
		86	92	noMNSLD
AXSXXX422	FOIN	59	98	noMNSLD
AXSXXX423	FOIN	82	271	noMNSLD
		61	103	noMNSLD
		56	296	noMNSLD
AXSXXX424	FOIN	45	262	noMNSLD
AXSXXX425	FOIN	80	273	noMNSLD
		82	100	noMNSLD
AXSXXX426	FOIN	70	255	noMNSLD
		71	258	noMNSLD
AXSXXX427	FOIN	90	269	noMNSLD
		73	108	noMNSLD
		77	92	noMNSLD
AXSXXX428	FOIN	88	107	noMNSLD
AXSXXX429	FOIN	89	274	noMNSLD
AXSXXX429	FOIN	35	4	noMNSLD

AXSXXX481	FOIN	86	314	mig 2 Cohn
AXSXXX483	FOIN	87	274	mig 2 Cohn
		88	297	mig 2 Cohn
AXSXXX485	FOIN	86	277	mig 2 Cohn
		88	224	mig 2 Cohn
AXSXXX486	FOIN	88	264	mig 2 Cohn
AXSXXX487	FOIN	72	89	mig 2 Cohn
AXSXXX488	FOIN	78	278	mig 2 Cohn
		76	271	mig 2 Cohn
		69	267	mig 2 Cohn
		73	279	mig 2 Cohn
		86	279	mig 2 Cohn
AXSXXX490	FOIN	84	249	mig 2 Cohn
		83	239	mig 2 Cohn
		85	70	mig 2 Cohn
AXSXXX491	FOIN	79	253	mig 2 Cohn
		86	67	mig 2 Cohn
		87	251	mig 2 Cohn
AXSXXX494	FOIN	72	257	mig 2 Cohn

Appendix 1 – All foliations and lineations

AXSXXX496	FOIN	78	226	CohnHILL
		88	109	CohnHILL
AXSXXX497	FOIN	77	214	CohnHILL
		73	217	CohnHILL
AXSXXX499	FOIN	71	251	CohnHILL
		64	274	CohnHILL
		66	246	CohnHILL
		76	225	CohnHILL
AXSXXX500	FOIN	70	239	CohnHILL
AXSXXX501	FOIN	77	270	CohnHILL
		87	237	CohnHILL
		87	86	CohnHILL
		83	254	CohnHILL
		77	253	CohnHILL
AXSXXX502	FOIN	74	230	CohnHILL
AXSXXX503	FOIN	76	224	CohnHILL
AXSXXX506	FOIN	68	226	CohnHILL
		62	217	CohnHILL
AXSXXX507	FOIN	73	236	CohnHILL
AXSXXX508	FOIN	72	254	CohnHILL
		79	226	CohnHILL
AXSXXX509	FOIN	64	246	CohnHILL
		58	198	CohnHILL
AXSXXX510	FOIN	61	239	CohnHILL
AXSXXX511	FOIN	79	74	CohnHILL
AXSXXX512	FOIN	64	238	CohnHILL
		66	239	CohnHILL
AXSXXX513	FOIN	69	235	CohnHILL
AXSXXX514	FOIN	88	251	CohnHILL
		87	254	CohnHILL
		81	250	CohnHILL
AXSXXX515	FOIN	89	296	CohnHILL
AXSXXX518	FOIN	82	238	CohnHILL
		73	118	CohnHILL
		84	223	CohnHILL
AXSXXX519	FOIN	60	207	CohnHILL
		66	197	CohnHILL
		57	205	CohnHILL
		62	209	CohnHILL
AXSXXX520	FOIN	69	146	CohnHILL
		71	226	CohnHILL
		59	169	CohnHILL
		60	165	CohnHILL
		82	258	CohnHILL
		79	249	CohnHILL
		80	195	CohnHILL
AXSXXX521	FOIN	73	258	CohnHILL
		70	290	CohnHILL
		63	197	CohnHILL
		61	245	CohnHILL
		70	220	CohnHILL

Appendix 1 – All foliations and lineations

AXSXXX522	FOIN	65	210	CohnHILL
		62	215	CohnHILL
AXSXXX525	FOIN	58	234	CohnHILL
AXSXXX526	FOIN	71	254	CohnHILL
AXSXXX530	FOIN	53	228	CohnHILL
		63	244	CohnHILL
		63	249	CohnHILL
		89	247	CohnHILL
		84	210	CohnHILL
AXSXXX531	FOIN	41	214	CohnHILL
		71	240	CohnHILL
AXSXXX532	FOIN	61	270	CohnSurr
		69	267	CohnSurr
		62	262	CohnSurr
AXSXXX533	FOIN	87	83	CohnSurr
		86	265	CohnSurr
AXSXXX534	FOIN	90	267	CohnSurr
		79	265	CohnSurr
		72	264	CohnSurr
		83	259	CohnSurr
AXSXXX536	FOIN	71	259	CohnSurr
		77	254	CohnSurr
AXSXXX537	FOIN	81	263	CohnSurr
		69	263	CohnSurr
AXSXXX551	FOIN	68	103	
AXSXXX552	FOIN	72	107	
AXSXXX555	FOIN	74	289	
AXSXXX607	FOIN	65	279	Minnie Hill
		69	279	
		65	269	
AXSXXX608	FOIN	73	281	Minnie Hill
		58	273	
AXSXXX609	FOIN	49	252	Minnie Hill
		54	246	
AXSXXX610	FOIN	57	263	Minnie Hill
		69	258	
AXSXXX611	FOIN	63	268	Minnie Hill
		64	267	
		63	265	
AXSXXX612	FOIN	67	275	Minnie Hill
		75	316	
AXSXXX613	FOIN	67	278	Minnie Hill
AXSXXX614	FOIN	43	271	Minnie Hill
		47	285	
AXSXXX615	FOIN	60	232	Minnie Hill
AXSXXX616	FOIN	52	290	Minnie Hill
		49	300	

Appendix 1 – All foliations and lineations

AXSXXX617	FOIN	67	298	Minnie Hill
AXSXXX618	FOIN	53	259	Minnie Hill
		51	272	
AXSXXX619	FOIN	51	295	Minnie Hill
		49	289	
		46	290	
AXSXXX620	FOIN	43	298	Minnie Hill
AXSXXX621	FOIN	59	270	Minnie Hill
AXSXXX622	FOIN	57	284	Minnie Hill
		61	280	
		52	288	
AXSXXX624	FOIN	63	283	Minnie Hill
AXSXXX625	FOIN	70	284	Minnie Hill
AXSXXX626	FOIN	57	271	Minnie Hill
		42	268	
		37	244	
		48	258	
		40	260	
		56	278	
		57	271	
		55	262	
AXSXXX627	FOIN	36	257	Minnie Hill
		37	244	
AXSXXX628	FOIN	51	276	Minnie Hill
		41	270	
AXSXXX629	FOIN	49	279	Minnie Hill
AXSXXX630	FOIN	56	273	Minnie Hill
		52	276	
AXSXXX631	FOIN	50	262	Minnie Hill
		52	260	
		49	246	
AXSXXX632	FOIN	69	254	Minnie Hill
		63	261	
AXSXXX633	FOIN	42	236	Minnie Hill
		28	236	
AXSXXX634	FOIN	55	240	Minnie Hill
		54	242	
AXSXXX635	FOIN	44	264	Minnie Hill
		44	258	
AXSXXX636	FOIN	49	276	Minnie Hill
		43	296	
AXSXXX637	FOIN	52	290	Minnie Hill
		52	298	
		60	306	
AXSXXX638	FOIN	54	294	Minnie Hill
		57	304	
AXSXXX639	FOIN	53	285	Minnie Hill
		60	285	
		52	276	
AXSXXX640	FOIN	45	291	Minnie Hill
		53	282	

Appendix 1 – All foliations and lineations

AXSXXX641	FOIN	49	298	Minnie Hill
		41	306	
AXSXXX642	FOIN	42	312	
AXSXXX643	FOIN	52	271	Minnie Hill
		57	289	
		53	272	
AXSXXX645	FOIN	53	267	Minnie Hill
		52	274	
AXSXXX647	FOIN	72	293	Minnie Hill
AXSXXX648	FOIN	73	298	Minnie Hill
AXSXXX649	FOIN	52	279	Minnie Hill
AXSXXX650	FOIN	49	278	Minnie Hill
AXSXXX652	FOIN	69	291	Minnie Hill
AXSXXX653	FOIN	69	291	Minnie Hill
AXSXXX654	FOIN	73	269	Minnie Hill
AXSXXX655	FOIN	78	270	Minnie Hill
AXSXXX656	FOIN	44	267	Minnie Hill
AXSXXX657	FOIN	57	279	Minnie Hill
AXSXXX658	FOIN	56	246	Minnie Hill
AXSXXX659	FOIN	48	276	Minnie Hill
AXSXXX660	FOIN	64	280	Minnie Hill
AXSXXX662	FOIN	65	284	Minnie Hill
AXSXXX430	FOIN	69	289	Minnie Hill
		79	280	Minnie Hill
AXSXXX431	FOIN	66	266	Minnie Hill
		58	270	Minnie Hill
		61	261	Minnie Hill
AXSXXX433	FOIN	52	287	Minnie Hill
		50	282	Minnie Hill
		60	304	Minnie Hill
AXSXXX434	FOIN	49	294	Minnie Hill
AXSXXX435	FOIN	41	320	Minnie Hill
		42	314	Minnie Hill
AXSXXX436	FOIN	45	310	Minnie Hill
AXSXXX437	FOIN	48	320	Minnie Hill
		40	299	Minnie Hill
		50	286	Minnie Hill
AXSXXX438	FOIN	52	286	Minnie Hill
		44	280	Minnie Hill
AXSXXX439	FOIN	76	284	Minnie Hill
AXSXXX440	FOIN	53	264	Minnie Hill
		45	282	Minnie Hill
AXSXXX441	FOIN	52	280	Minnie Hill
		69	267	Minnie Hill
		50	270	Minnie Hill
		44	284	Minnie Hill
AXSXXX442	FOIN	39	299	Minnie Hill
AXSXXX443	FOIN	41	296	Minnie Hill
AXSXXX444	FOIN	50	281	Minnie Hill
AXSXXX445	FOIN	61	264	Minnie Hill

Appendix 1 – All foliations and lineations

AXSXXX446	FOIN	61	250	Minnie Hill
		63	258	Minnie Hill
		57	250	Minnie Hill
AXSXXX447	FOIN	62	277	Minnie Hill
		61	281	Minnie Hill
AXSXXX448	FOIN	60	270	Minnie Hill
AXSXXX449	FOIN	65	264	Minnie Hill
		63	278	Minnie Hill
AXSXXX450	FOIN	89	261	Minnie Hill
		71	276	Minnie Hill
AXSXXX451	FOIN	66	250	Minnie Hill
		61	259	Minnie Hill
		54	264	Minnie Hill
		64	274	Minnie Hill
AXSXXX452	FOIN	62	274	Minnie Hill
		45	284	Minnie Hill
		67	273	Minnie Hill
AXSXXX453	FOIN	44	270	Minnie Hill
		48	256	Minnie Hill
AXSXXX454	FOIN	48	256	Minnie Hill
AXSXXX455	FOIN	55	271	Minnie Hill
		44	252	Minnie Hill
AXSXXX456	FOIN	52	278	Minnie Hill
		43	264	Minnie Hill
AXSXXX457	FOIN	44	259	Minnie Hill
AXSXXX458	FOIN	63	279	Minnie Hill
AXSXXX459	FOIN	58	310	Minnie Hill
		56	300	Minnie Hill
		57	311	Minnie Hill
		54	290	Minnie Hill
AXSXXX460	FOIN	45	275	Minnie Hill
AXSXXX461	FOIN	43	270	Minnie Hill
AXSXXX462	FOIN	46	309	Minnie Hill
		57	316	Minnie Hill
		38	306	Minnie Hill
		59	277	Minnie Hill
AXSXXX464	FOIN	51	272	Minnie Hill
AXSXXX465	FOIN	52	287	Minnie Hill
		43	269	Minnie Hill
AXSXXX466	FOIN	50	264	Minnie Hill
		59	244	Minnie Hill
		44	274	Minnie Hill
AXSXXX467	FOIN	40	270	Minnie Hill
		43	276	Minnie Hill
		50	270	Minnie Hill
AXSXXX468	FOIN	45	260	Minnie Hill
AXSXXX470	FOIN	53	257	Minnie Hill
		44	267	Minnie Hill
		42	251	Minnie Hill
		62	280	Minnie Hill
AXSXXX471	FOIN	52	296	Minnie Hill

Appendix 1 – All foliations and lineations

		60	303	Minnie Hill
		53	292	Minnie Hill
		50	298	Minnie Hill
AXSXXX473	FOIN	54	299	Minnie Hill
		49	291	Minnie Hill
AXSXXX474	FOIN	60	287	Minnie Hill
AXSXXX475	FOIN	47	260	Minnie Hill
		45	260	Minnie Hill
AXSXXX476	FOIN	49	289	Minnie Hill
AXSXXX477	FOIN	50	270	Minnie Hill
		45	268	Minnie Hill

All lineations:

SITEID	STRUCTYPEID	L_AZIMUTH	PLUNGE
AXSXXX310	LINU	306	19
		322	30
AXSXXX311	LINU	339	6
AXSXXX313	LINU	297	23
AXSXXX314	LINU	344	12
		340	9
AXSXXX325	LINU	348	39
AXSXXX337	LINU	8	35
		12	41
AXSXXX338	LINU	58	38
AXSXXX339	LINU	353	49
AXSXXX340	LINU	340	26
AXSXXX341	LINU	344	19
		345	20
		347	20
AXSXXX342		358	2
		1	9
AXSXXX343	LINU	1	20
AXSXXX344	LINU	342	13
		337	15
AXSXXX345	LINU	356	20
AXSXXX346	LINU	13	33
		9	34
AXSXXX347	LINU	5	8
AXSXXX349	LINU	17	1
		204	3
		192	1
AXSXXX350	LINU	38	25
AXSXXX354	LINU	357	14
AXSXXX355	LINU	2	4
AXSXXX357	LINU	27	13
AXSXXX360	LINU	22	6

Appendix 1 – All foliations and lineations

AXSXXX361	LINU	28	42
AXSXXX362	LINU	19	17
AXSXXX367	LINU	30	12
		8	5
		12	10
AXSXXX368	LINU	38	3
AXSXXX369	LINU	25	6
AXSXXX370	LINU	11	1
AXSXXX371	LINU	4	12
AXSXXX372	LINU	14	5
AXSXXX373	LINU	20	6
AXSXXX374	LINU	22	2
AXSXXX377	LINU	102	27
		102	27
AXSXXX378	LINU	9	23
		3	7
AXSXXX381	LINU	61	16
		97	19
AXSXXX382	LINU	63	43
AXSXXX384	LINU	24	14
AXSXXX386	LINU	30	24
AXSXXX392	LINU	15	12
AXSXXX396	LINU	23	33
AXSXXX399	LINU	23	10
AXSXXX400	LINU	10	6
AXSXXX401	LINU	102	20
		105	7
AXSXXX403	LINU	7	22
		7	14
AXSXXX405	LINU	3	9
AXSXXX406	LINU	22	28
		28	29
AXSXXX407	LINU	23	10
		27	8
AXSXXX412	LINU	25	10
		25	9
AXSXXX414	LINU	20	13
AXSXXX421	LINU	28	21
AXSXXX422	LINU	28	19
		23	22
AXSXXX423	LINU	3	25
		5	7
AXSXXX424	LINU	344	22
AXSXXX425	LINU	351	32
AXSXXX426	LINU	328	50
		322	55
AXSXXX429	LINU	4	35
AXSXXX430	LINU	356	40
		280	79
AXSXXX431	LINU	337	33
		346	24

Appendix 1 – All foliations and lineations

AXSXXX433	LINU	334	41
AXSXXX434	LINU	324	42
AXSXXX435	LINU	310	39
		345	42
AXSXXX436	LINU	306	47
AXSXXX437	LINU	345	31
		341	42
AXSXXX438	LINU	334	39
		318	41
AXSXXX439	LINU	345	32
AXSXXX440	LINU	316	37
AXSXXX441	LINU	340	38
		324	29
AXSXXX442	LINU	323	35
AXSXXX443	LINU	330	37
		327	44
AXSXXX444	LINU	319	38
AXSXXX445	LINU	320	32
AXSXXX446	LINU	318	34
		327	30
		304	46
AXSXXX447	LINU	4	20
AXSXXX449	LINU	317	39
AXSXXX455	LINU	181	17
		175	4
		166	13
AXSXXX456	LINU	349	8
		341	4
		358	8
AXSXXX457	LINU	356	4
		350	9
		1	16
		334	14
AXSXXX461	LINU	329	18
AXSXXX462	LINU	255	29
		245	30
		231	28
AXSXXX464	LINU	335	22
AXSXXX465	LINU	311	38
		296	50
AXSXXX467	LINU	339	22
		338	21
AXSXXX468	LINU	348	20
		351	19
AXSXXX470	LINU	324	20
		337	19
AXSXXX471	LINU	27	19
		8	18
AXSXXX473	LINU	19	3
AXSXXX475	LINU	204	25
AXSXXX476	LINU	18	18

Appendix 1 – All foliations and lineations

AXSXXX477	LINU	296	4
		295	0
AXSXXX481	LINU	14	43
AXSXXX483	LINU	356	38
AXSXXX485	LINU	3	48
AXSXXX486	LINU	351	37
AXSXXX488	LINU	17	38
		7	32
		23	42
AXSXXX496	LINU	303	62
AXSXXX498	LINU	20	66
AXSXXX499	LINU	290	61
		20	66
AXSXXX500	LINU	308	52
AXSXXX500	LINU	158	66
AXSXXX500	LINU	156	28
AXSXXX502	LINU	283	60
		191	59
AXSXXX506	LINU	18	62
		173	51
		185	43
		164	44
AXSXXX507	LINU	173	51
AXSXXX508	LINU	156	54
		159	52
AXSXXX509	LINU	191	55
		161	52
AXSXXX510	LINU	166	29
		200	61
AXSXXX512	LINU	168	52
		193	45
AXSXXX513	LINU	163	33
AXSXXX514	LINU	340	12
		316	37
		334	42
AXSXXX518	LINU	149	49
AXSXXX519	LINU	217	63
		236	52
AXSXXX525	LINU	198	57
AXSXXX530	LINU	243	43
		153	59
AXSXXX531	LINU	203	39
AXSXXX532	LINU	345	24
		334	28
		347	15
AXSXXX533	LINU	351	15
AXSXXX534	LINU	346	33
		337	42
AXSXXX536	LINU	340	31
		338	21
AXSXXX537	LINU	345	31

Appendix 1 – All foliations and lineations

		344	31
		345	31
AXSXXX556	LINU	31	10
		25	11
AXSXXX557	LINU	7	14
AXSXXX558	LINU	18	13
AXSXXX559	LINU	31	11
AXSXXX560	LINU	32	12
		24	11
		38	8
AXSXXX561	LINU	22	14
AXSXXX562	LINU	29	5
AXSXXX563	LINU	15	29
AXSXXX565	LINU	19	4
AXSXXX567	LINU	22	10
AXSXXX568	LINU	12	6
		21	19
AXSXXX569	LINU	13	21
AXSXXX571	LINU	16	9
AXSXXX572	LINU	7	9
AXSXXX573	LINU	12	8
AXSXXX578	LINU	24	13
AXSXXX579	LINU	21	10
AXSXXX582	LINU	12	19
AXSXXX583	LINU	354	34
AXSXXX594	LINU	39	16
AXSXXX595	LINU	19	12
AXSXXX596	LINU	25	8
		22	7
AXSXXX599	LINU	19	4
AXSXXX600	LINU	23	4
		47	7
AXSXXX602	LINU	26	12
AXSXXX611	LINU	336	45
AXSXXX614	LINU	344	44
		329	31
AXSXXX615	LINU	339	44
AXSXXX616	LINU	354	32
AXSXXX618	LINU	332	20
AXSXXX619	LINU	343	39
		351	32
AXSXXX620	LINU	352	26
AXSXXX621	LINU	342	22
AXSXXX622	LINU	357	26
		1	21
AXSXXX625	LINU	354	41
AXSXXX635	LINU	233	33
		204	18
		214	39
AXSXXX636	LINU	237	32
AXSXXX637	LINU	348	50

Appendix 1 – All foliations and lineations

AXSXXX639	LINU	0	20
		346	31
AXSXXX640	LINU	342	33
		354	23
AXSXXX641	LINU	200	14
AXSXXX643	LINU	195	24
AXSXXX646	LINU	338	22
AXSXXX648	LINU	213	8
AXSXXX649	LINU	347	31
AXSXXX651	LINU	6	18
AXSXXX656	LINU	344	14
AXSXXX657	LINU	353	23
AXSXXX658	LINU	322	29
AXSXXX659	LINU	345	23
		352	22
AXSXXX662	LINU	353	36

RECORD 2009/24

AGE CONSTRAINTS AND STRUCTURE OF THE COHN HILL SHEAR ZONE, WESTERN MUSGRAVE BLOCK, WESTERN AUSTRALIA

This Record is published in digital format (PDF) and is available online at: www.dmp.wa.gov.au/GSWApublications.
Laser-printed copies can be ordered from the Information Centre for the cost of printing and binding.

Further details of geological publications and maps produced by the Geological Survey of Western Australia can be obtained by contacting:

Information Centre
Department of Mines and Petroleum
100 Plain Street
EAST PERTH, WESTERN AUSTRALIA 6004
Phone: (08) 9222 3459 Fax: (08) 9222 3444
www.dmp.wa.gov.au/GSWApublications

SEN